



# Spatiotemporal evolution and driving mechanisms of desertification on the Mongolian Plateau

Shuxing Xu<sup>a,b</sup>, Juanle Wang<sup>a,b,c,\*</sup>, Ochir Altansukh<sup>d</sup>, Togtokh Chuluun<sup>e</sup>

<sup>a</sup> State Key Laboratory of Resources and Environmental Information System, Institute of Geographic Sciences and Natural Resources Research, Chinese Academy of Sciences, Beijing 100101, China

<sup>b</sup> University of Chinese Academy of Sciences, Beijing 100049, China

<sup>c</sup> Jiangsu Center for Collaborative Innovation in Geographical Information Resource Development and Application, Nanjing 210023, China

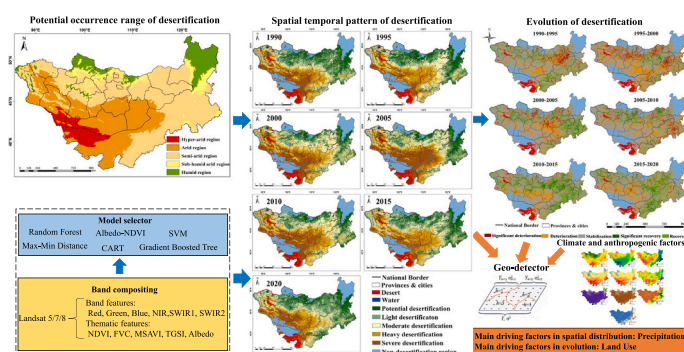
<sup>d</sup> Environmental Engineering Laboratory, Department of Environment and Forest Engineering, National University of Mongolia, Ulaanbaatar 14201, Mongolia

<sup>e</sup> Institute for Sustainable Development, National University of Mongolia, Ulaanbaatar 14201, Mongolia

## HIGHLIGHTS

- Gradient boosted tree algorithm is adaptable to desertification monitoring.
- 30-meter resolution desertification map of the entire Mongolian plateau was firstly retrieved from 1990 to 2020.
- The year 2010 showed transition to land restoration in Mongolian Plateau.
- Quantifying the drivers of the distribution and evolution of desertification on the Mongolian Plateau, respectively.
- Explaining the heterogeneity of desertification evolution and driving mechanisms in Inner Mongolia, China and Mongolia.

## GRAPHICAL ABSTRACT



## ARTICLE INFO

Editor: Ouyang Wei

### Keywords:

Desertification  
Remote sensing inversion  
Machine learning  
Climate change  
Human activities  
Mongolia Plateau

## ABSTRACT

Desertification poses a severe ecological and environmental challenge in the Mongolian Plateau (MP). It is difficult to quantify desertification distribution using unified indicators in the entire MP, because of its complex physical geographic conditions and various climatic zones covered. To accurately address this challenge, the spatial distribution of desertification at a 30-m resolution from 1990 to 2020 were mapped in this study. The desertification potential occurrence zone was identified by using a moisture index on the MP firstly. The feature space model and five machine learning models were constructed to make the map based on Google Earth Engine and Landsat data. The spatiotemporal distribution of desertification were further analyzed, and the dominant drivers of desertification distribution and evolution were identified using Geodetector model. The results indicate that the potential occurrence area of desertification accounted for 83.88 % of the total land area. The gradient boosted tree model for desertification assessment has the best performance with the highest overall accuracy of 88.18 %. The year 2010 marked a pivotal transition from land degradation to land restoration in the MP. Between 2010 and 2020, desertified land continued to deteriorate extensively in the southern Mongolia, while Inner Mongolia, China, essentially entered a full recovery phase. Precipitation and land use emerged as the

\* Corresponding author at: State Key Laboratory of Resources and Environmental Information System, Institute of Geographic Sciences and Natural Resources Research, Chinese Academy of Sciences, Beijing, 100101, China.

E-mail address: [wangjl@igsnrr.ac.cn](mailto:wangjl@igsnrr.ac.cn) (J. Wang).

<https://doi.org/10.1016/j.scitotenv.2024.173566>

Received 2 January 2024; Received in revised form 25 May 2024; Accepted 25 May 2024

Available online 31 May 2024

0048-9697/© 2024 Elsevier B.V. All rights are reserved, including those for text and data mining, AI training, and similar technologies.

primary drivers of the spatial distribution of desertification on the Mongolian Plateau and Mongolia, with potential evapotranspiration and precipitation influencing the distribution of desertification in Inner Mongolia, China. Land use change was the primary driver of desertification evolution on the MP and Mongolia. This study constructs an indicator system and methodology suitable for desertification monitoring on the MP, addresses the lack of refined desertification data over a long time series, and provides scientific reference for decision-making support in combating desertification in this region, and other large arid and semi-arid areas in the world.

## 1. Introduction

Desertification is a critical environmental and socioeconomic challenge in arid and semi-arid areas, characterized by the continuous decline or loss of biodiversity or land productivity (Xiao et al., 2006; Shao et al., 2023). Globally, over 20 % of arable land, 30 % of forests, and 10 % of grasslands are undergoing degradation, affecting approximately one-sixth of the population (Christian and Dhinwa, 2018; Linnér and Messing, 2012; Berdugo et al., 2017). Desertification increases the severity and frequency of sandstorms, food shortages, and poverty, posing threats to human health and well-being (Liu et al., 2020; Alherbawi et al., 2022). Recognizing the urgency, the United Nations General Assembly incorporated combating desertification as one of 17 sustainable development goals (SDGs) in 2015, within the 2030 Agenda for Sustainable Development (2030 Agenda) (United Nations, 2015). SDGs Target 15.3 explicitly focuses on combat desertification, restoring degraded land and soil, and striving to achieve a land degradation-neutral world by 2030. The risk of desertification in drylands has intensified owing to the escalating impacts of climate change (Huang et al., 2019; IPCC, 2019). Thus, it is imperative to scientifically quantify the fine spatiotemporal evolution and driving mechanism of desertification, providing data and theoretical support for policy formulation to combat desertification and achieve the goal of Land Degradation Neutrality (LDN).

Desertification monitoring primarily involves field surveys and remote sensing (Zhang and Huisingh, 2018; Rivera-Marin et al., 2022). While field investigations have the highest accuracy, they are impractical for large-scale desertification monitoring due to the significant demands on labor, time, and financial resources (Zhao et al., 2019). Compared to traditional ground-based monitoring, the scientific, efficient, accurate, and automated features of remote sensing technology render it the preferred choice for global and regional desertification monitoring over long time series (Zhang et al., 2021). Advancements in remote sensing observation technology and cloud computing platforms have facilitated the gradual application of high-resolution remote sensing images (10–30 m resolution) to analyze spatiotemporal patterns and the precise evolution of desertification on a large regional scale (Meng et al., 2021; Xu et al., 2023), marking significant progress compared to earlier research conducted at a scale of 250–1000 m (Duan et al., 2019). Targeting such high-resolution remote sensing images, feature space models, and machine learning algorithms has become a research hotspot for rapid long-term monitoring of desertification on a large regional scale (Fan et al., 2020; Meng et al., 2021; Wei et al., 2020). However, owing to the complexity of desertification processes, the performances of feature space models and machine learning algorithms exhibit considerable variability under distinct geographic conditions (Wei et al., 2018; Jiang et al., 2023; Feng et al., 2022; Zhao et al., 2023). Therefore, for precise large-scale desertification information extraction, synthesizing the performance of multiple feature space models and machine learning algorithms is necessary to enhance the accuracy of desertification monitoring (Wang et al., 2023b).

Desertification is the process of land degradation in arid, semiarid and dry sub-humid areas resulting from climate variations and human activities (UNCCD, 1994). Climate influences the extent and severity of desertification by altering the spatiotemporal distribution of precipitation, temperature, and wind (Ding and Hao, 2021). Irrational human activities including population explosion, aggressive mining,

overgrazing, and the expansion of arable land, contribute the destruction of vegetation and soil erosion, directly exacerbating desertification (Feng et al., 2015; Bardgett et al., 2021; Zhou et al., 2019). Ecological restoration policies, such as the Three Norths Shelter Forest Program (TNSFP) and the grazing policy, are recognized as important drivers of desertification dynamics, affecting the desertification process by affecting land use change (Turner et al., 2023; Liu et al., 2020). Various quantitative methods such as correlation analysis, generalized linear models, principal component analysis, and random forest models have been employed to assess the contribution of individual natural and social factors to desertification distribution (Jiang et al., 2023; Meng et al., 2021; Wang et al., 2020; Xie et al., 2015). The impact of anthropogenic activities and natural factors on desertification can also be quantified by assessing changes in indicators such as net primary productivity (Zhao et al., 2023; Zhang et al., 2022). However, this method relies on 250- and 500-m MODIS datasets with coarse spatial resolution, resulting in highly uncertain results for sparsely vegetated areas (Li et al., 2015). Concurrently, the contributions of individual climatic and anthropogenic factors to desertification cannot be captured using this method. In contrast, based on high-resolution desertification data, the Geo-detector model can quantitatively assess the impact of various factors and further explore the interaction mechanisms of climatic and anthropogenic factors on desertification (Qi et al., 2023; Wang et al., 2023c).

The Mongolian Plateau (MP), one of the most arid zones in the northern hemisphere, is highly susceptible to land degradation due to climate change and anthropogenic activities. Mongolia is a global desertification hotspot, with 76.8 % and 76.9 % of its total territory desertified in 2015 and 2020, respectively (Chan et al., 2023; Wei et al., 2018). Adjacent to Mongolia, Inner Mongolia, China, is one of the regions most seriously affected by desertification in China (Zhang and Huisingh, 2018). Climate variation, overgrazing and other irrational human activities have further exacerbated desertification on the MP. In recent years, strong dust storms have swept through Mongolia, causing significant human casualties and economic losses, and severely affecting most of Northeast Asia (Zhang et al., 2023). Desertification of the MP poses a significant challenge to achieving LDN. Additionally, as a representative arid steppe zone in the Eurasian continent, desertification directly threatens regional ecological security and the well-being of the local population.

However, most current studies on refined desertification monitoring in the MP focused on Inner Mongolia (China), Mongolia, or smaller localized case studies (Duan et al., 2019; Meng et al., 2021; Xu et al., 2023; Zhao et al., 2023) and fail to grasp the refined evolution of desertification on the entire MP from a global and holistic perspective. Additionally, there is a deficiency in long-term time series and highly detailed desertification data, hindering a comprehensive and accurate assessment of desertification evolution. Low-resolution desertification data include numerous mixed pixels, leading to high uncertainty in the results (Wang et al., 2023b) and, impeding the precise formulation and implementation of desertification control strategies. Finally, research on the mechanisms driving desertification across the MP is limited. Previous studies conducted in Mongolia and Inner Mongolia have primarily concentrated on a single desertification spatial distribution pattern (Meng et al., 2021) or a coarse-grained analysis of desertification evolution mechanisms, which have not adequately elucidated the contributions of natural and anthropogenic factors to the spatial distribution pattern and evolution of desertification, nor have they explored the

impact of interactions between factors.

To address this scientific hurdle, this study aimed to enhance the nuanced understanding of the evolutionary characteristics of global desertification on the MP by applying big data and artificial intelligence technologies. It also sought to quantitatively identify the driving mechanisms of the spatial distribution and evolution of desertification at different regional scales. This study provides a detailed and reliable data base for the delineation of key areas for desertification control on the MP, and offers a reference for quantitative analysis of desertification-driven mechanisms.

## 2. Material and methods

### 2.1. Study area

This study focused on the core area of the Mongolian Plateau (87°43'–126°04'E, 37°22'–53°20'N), encompassing the Inner Mongolia Autonomous Region of China and Mongolia. The total area of the study region is approximately 2,749,500 km<sup>2</sup>, comprising 1,183,000 km<sup>2</sup> of Inner Mongolia and 1,566,500 km<sup>2</sup> of Mongolia (Fig. 1). The topography exhibits complexity and variation, gradually descending from northwest to southeast, with an average elevation of 1580 m. Mountains dominate the northwest, large scale hills are prevalent in the center and east, and the Gobi Desert extends across the southwest. The MP, situated deep inland, experiences a typical temperate continental climate, with low precipitation and significant temporal and spatial variations (Zheng

et al., 2023). The climate distribution pattern transitions from a sub-humid arid zone in the north and east to semi-arid, arid, and hyper-arid zones in the southwest. The regional ecological environment is fragile, and vegetation distribution follows a clear banding pattern, with eight types from north to south: coniferous forests, mixed forests, deciduous forests, forest grasslands, meadow grasslands, typical grasslands, desert grasslands, and deserts. Clear disparities in socioeconomic development exist between China and Mongolia, with the populations of Inner Mongolia, China consistently representing a significant proportion of the MP, averaging 90 % over the last 20 years (Chan et al., 2023). Animal husbandry constitutes the primary economic foundation for Inner Mongolia, China, and Mongolia, whereas mining is the principal mode of economic development in Mongolia (Liang et al., 2021).

### 2.2. Data sources

Landsat 5/7/8 imagery served as the primary remote sensing data for depicting the 30-m resolution desertification distribution on the MP in 1990, 1995, 2000, 2005, 2010, 2015, and 2020. Based on the Google Earth Engine (GEE), clouds, cloud shadows, and perennial snow were removed from each original image using quality assessment bands generated by the CFMASK algorithm. The normalized difference vegetation index (NDVI) maximum synthesis method was used to acquire high-quality images of the entire MP, showcasing optimal vegetation-growth conditions year round. Simultaneously, the global surface water dataset from the Joint Research Center (Pekel et al., 2016) was

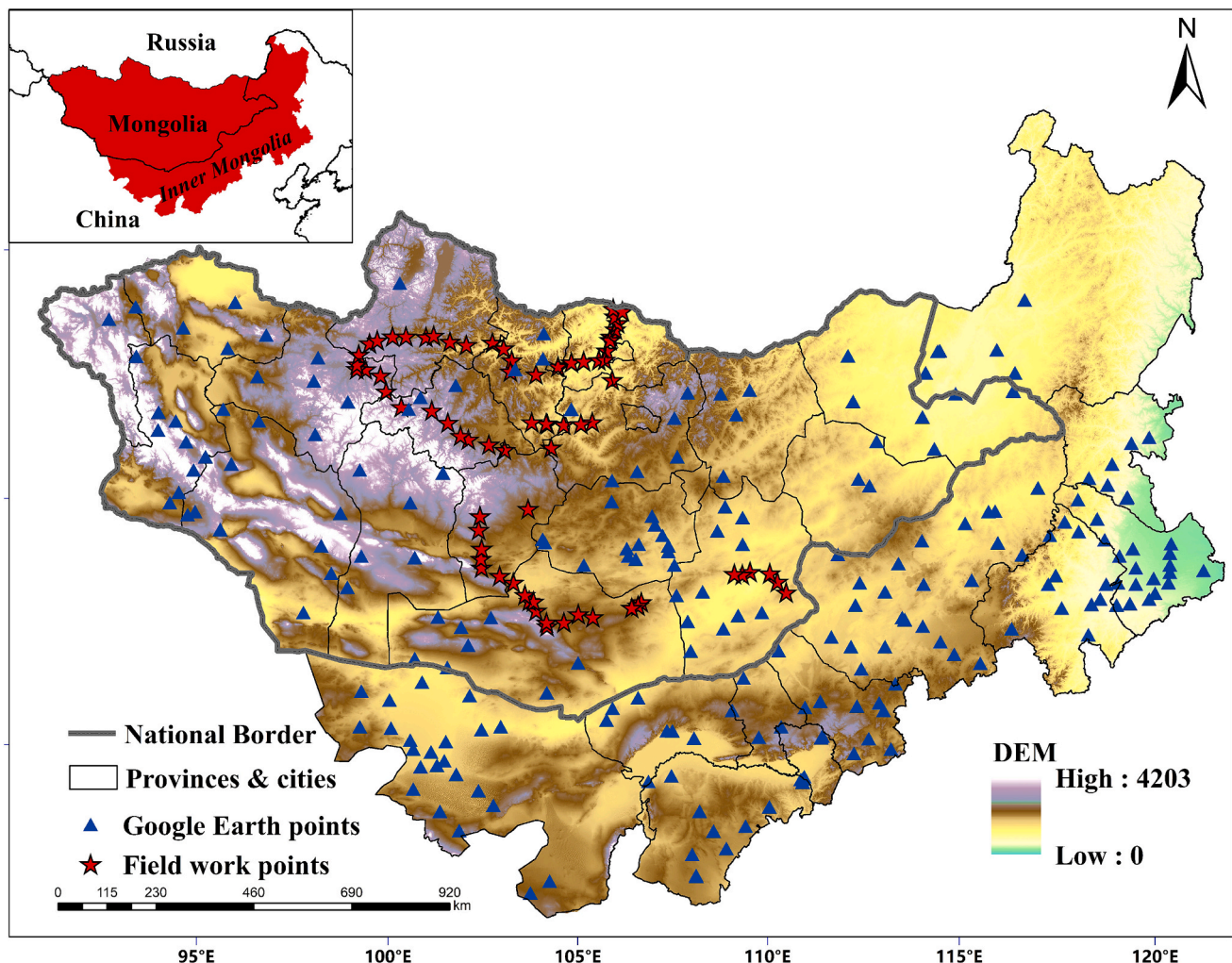


Fig. 1. The study area and the distribution of desertification sample points.



utilized to eliminate water bodies, thereby enhancing the accuracy of the desertification inversion results.

Table 1 shows details of the 12 natural and human factors used in this study, including data sources, abbreviation, resolution, units, and websites. We reclassified the classification system of the Land use/cover products (Wang et al., 2022; Xu et al., 2023) into 6 land use types (LU), including forest, grassland, cropland, bare land, sandy land, and others. Meanwhile, a total of four periods of LU conversion in the MP from 2000 to 2020 were obtained by using Arcgis.

2.3. Methods

In this study, we initially determined the potential range of desertification occurrence on the MP based on precipitation and potential evapotranspiration data. Subsequently, all Landsat images of the growing season (June–September) were filtered on GEE with cloud masking and quality screening, and NDVI maximum synthesis was utilized to obtain the images with the best annual vegetation growth conditions. These synthesized images were then used to calculate vegetation and soil indicators, and which were combined with Landsat's original spectral information to map the distribution of desertification using machine learning methods. Finally, we analyzed the spatial and temporal evolution of desertification on the MP over the last 30 years, and further explored the driving mechanisms of desertification at different regional scales on the Mongolian Plateau using Geodetector models. The specific technical process is shown in Fig. 2.

2.3.1. Determination of the potential occurrence extent of desertification in the MP

Desertification refers to land degradation caused by various factors, including changes in climate variability and anthropogenic activities in arid, semi-arid, and dry subhumid areas, characterized by a moisture index (MI) ranging from 0.05 to 0.65 (UNCCD, 1994). The MP is geographically complex, encompassing several climatic regions. According to the climate zoning sub-thresholds established by the United Nations Convention to Combat Desertification (UNCCD, 1994), the MP was categorized into five climate zones: hyper-arid ( $MI < 0.05$ ), arid ( $0.05 < MI < 0.2$ ), semi-arid ( $0.2 < MI < 0.5$ ), sub-humid semi-arid ( $0.2 < MI < 0.65$ ), and humid ( $0.65 < MI$ ). This categorization delineates the potential occurrence range of desertification on the MP, where MI is the ratio of the PRE to the PET.

2.3.2. Desertification information extraction methods

(1) Classification standards for desertification on the MP

Based on previous studies (Fan et al., 2020; Meng et al., 2021) and a field survey of the MP, desertification was categorized into five classes: severe, heavy, moderate, light, and potential desertification. With the field survey, we obtained information on land cover type, soil moisture, soil conductivity, soil grain size, vegetation cover, and the surrounding landscape condition of the field sites to comprehensively and accurately assess the desertification degree of the field survey sites. Table 2 presents landscape photographs and grading criteria for various degrees of desertification. Following the established desertification classification standards, 922 machine learning sample points for desertification were selected using high-resolution Google Earth imagery with the assistance of land-cover data on the MP. Combined with 78 field sites, a total of 1000 desertification sample points were compiled with 70 % allocated for model training and 30 % for model validation. The distribution of the sampling points is shown in Fig. 1.

(2) Desertification characterization indicators

Vegetation and soil conditions currently serve as the primary characteristic indicators for monitoring the degree of desertification through large-scale remote sensing. Vegetation is highly sensitive to changes in topography, geomorphology, soil, hydrological conditions, and climate, making it one of the most reliable indicators of desertification degree (Guo et al., 2022). The depletion of soil nutrients is the most severe consequence of desertification. In this study, five desertification indicators were selected: vegetation cover (FVC), NDVI, modified soil-adjusted vegetation index (MSAVI), albedo, and topsoil grain size index (TGSI). The NDVI is a common parameter used to characterize the growth and health of vegetation. In sparsely vegetated areas, the NDVI is less effective at characterizing vegetation conditions due to soil background interference. Consequently, the MSAVI was introduced to address this limitation (Huete, 1988). MSAVI can effectively mitigate the influence of the soil background, as it considers the fundamental soil line. FVC is an important index that reflects vegetation cover and can be used to evaluate land-use status and ecological environment quality (Li et al., 2016). Albedo is a comprehensive representation of soil moisture and nutrients. TGSI can be used to characterize the coarseness and fineness of soil particles (Xu et al., 2023). The remote sensing inversion formulas and bands used for the five vegetation and soil indicators are as follows:

Table 1  
Detailed information on 12 natural and human factors.

Data	Source	Abbreviation	Units	Resolution	Websites
Precipitation	TerraClimate dataset (Abatzoglou et al., 2018)	PRE	mm	~4 km	<a href="https://climatedataguide.ucar.edu/">https://climatedataguide.ucar.edu/</a>
Monthly maximum temperature		TMMN	°C		
Monthly minimum temperature		TMMX	°C		
Soil moisture		SM	°C		
Palmer drought index		PDSI	/		
Potential evapotranspiration		PET	mm		
Vapor pressure deficit	Shuttle Radar Topography Mission V3 the Institute of Geographic Sciences and Natural Resources, the Chinese Academy of Sciences	VPD	kPa	30 m	<a href="https://www.usgs.gov/">https://www.usgs.gov/</a> China: <a href="https://data.tpdc.ac.cn/home">https://data.tpdc.ac.cn/home</a> Mongolia: <a href="https://figshare.com/">https://figshare.com/</a>
Wind speed		WS	m/s		
Digital elevation model		DEM	m		
Land use/cover		/	/		
Livestock		LIVEST	thous. head		
Population		POP	person		
	Provincial statistical yearbooks of China; The Mongolian Statistical Office			Statistical data	China: <a href="http://tj.nmg.gov.cn/datashow/pubmgr/publishmanage.htm?m=queryPubData&amp;procode=0003&amp;cn=A017">http://tj.nmg.gov.cn/datashow/pubmgr/publishmanage.htm?m=queryPubData&amp;procode=0003&amp;cn=A017</a> Mongolia: <a href="http://www.1212.mn/en">http://www.1212.mn/en</a>



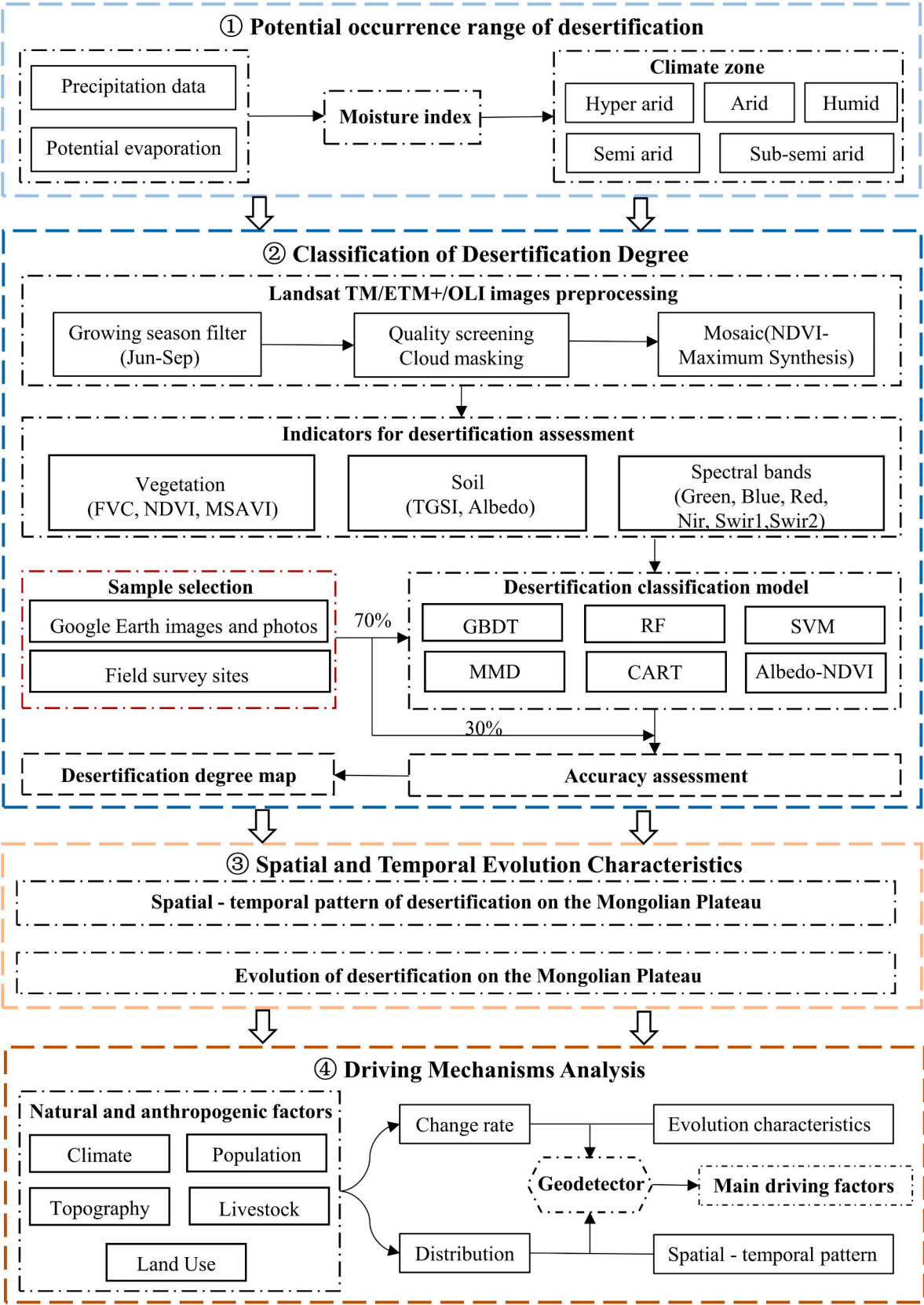
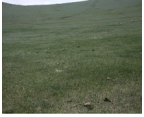






Fig. 2. The technical flowchart.

**Table 2**  
Landscape photographs and grading criteria for desertification on the MP.

Desertification degree	Landscape photos	Surface features	Vegetation cover /%
Potential		Dominated by forests and high-cover grasslands	> 65
Light		Inhibition of vegetation growth and emergence of poisonous weeds	50–65
Moderate		Low canopy emergence and sparse vegetation growth	10–50
Heavy		Vegetation patchiness disappears and the land begins to be sandy and accompanied by the growth of sandy vegetation	1–10
Severe		Loss of land productivity and regional vegetation, dominated by barren and sands.	< 1

$$\text{NDVI} = (\text{B}_{\text{nir}} - \text{B}_{\text{red}}) / (\text{B}_{\text{nir}} + \text{B}_{\text{red}}) \quad (1)$$

$$\text{FVC} = (\text{NDVI} - \text{NDVI}_{\text{soil}}) / (\text{NDVI}_{\text{veg}} + \text{NDVI}_{\text{soil}}) \quad (2)$$

$$\text{MSAVI} = \left( 2\text{B}_{\text{nir}} + 1 - \sqrt{(2\text{B}_{\text{nir}} + 1)^2 - 8(\text{B}_{\text{nir}} - \text{B}_{\text{red}})} \right) / 2 \quad (3)$$

$$\text{TGSI} = (\text{B}_{\text{red}} - \text{B}_{\text{blue}}) / (\text{B}_{\text{red}} + \text{B}_{\text{blue}} + \text{B}_{\text{green}}) \quad (4)$$

$$\text{Albedo} = 0.356\text{B}_{\text{blue}} + 0.13\text{B}_{\text{red}} + 0.373\text{B}_{\text{nir}} + 0.085\text{B}_{\text{swir1}} + 0.072\text{B}_{\text{swir2}} - 0.0018 \quad (5)$$

where  $\text{B}_{\text{red}}$ ,  $\text{B}_{\text{blue}}$ ,  $\text{B}_{\text{green}}$ ,  $\text{B}_{\text{nir}}$ ,  $\text{B}_{\text{swir1}}$ , and  $\text{B}_{\text{swir2}}$  are the reflectance of the red, blue, green, near-infrared, and shortwave infrared bands, respectively.  $\text{NDVI}_{\text{soil}}$  and  $\text{NDVI}_{\text{veg}}$  are the NDVI value of pure bare soil and pure vegetation, respectively.

### (3) Machine learning and feature space models

Utilizing the GEE platform, we conducted a thorough comparison of five machine learning models and a feature space model to map the desertification distribution across the Mongolian Plateau. These models comprised CART, SVM, RF, GBDT, MMD, and the Albedo-NDVI feature space model. Table 3 summarizes the principles of each model.

#### 2.3.3. Accuracy assessment methods

The confusion matrices were employed to quantify the accuracy of various machine learning and feature space models in extracting desertification information. It consisted of four main evaluation indicators: the overall accuracy (OA), Kappa coefficient, the producer's accuracy (PA), and the user's accuracy (UA). OA is the ratio of the sum

**Table 3**  
The principles of the desertification monitoring models.

Models	Basic principles
Albedo-NDVI	The NDVI and Albedo have a strong negative linear correlation between different desertified lands. By dividing the feature space in the vertical direction of the desertification trend, different desertification degrees can be distinguished (Wei et al., 2018).
MMD	Max-Min Distance method is a trial-based class clustering algorithm. It is based on the Euclidean distance and takes the object as far away as possible as the clustering center, which can intelligently determine the number of seeds of the first-trial clustering and improve the efficiency of dividing the first-trial dataset (Wei et al., 2017).
CART	Classification and Regression Tree is a binary recursive model based on a tree structure. After dividing the original sample into two sub-samples, the bisection of the sub-samples continues until they cannot be split. It is characterized by easy understanding and high computational efficiency (Li et al., 2020).
RF	Random Forest is an integrated model consisting of many decision trees. Its function idea is to build multiple small decision trees using different subsample sets and feature attributes when training data is input into the model and then combine them into a more powerful model (Belgiu and Drăguț, 2016).
SVM	Based on the structural minimization risk principle in statistical learning theory, support vector machines achieve data classification by finding an optimal hyperplane (Xu et al., 2015).
GBDT	Gradient Boosted Tree is an iterative decision tree algorithm that consists of multiple decision trees, and the conclusions of all the trees are accumulated to make the final answer. It is a boosting algorithm (Xing et al., 2022).

of correctly classified pixels to the total number of pixels. The Kappa coefficient is a statistical measure to assess the overall reliability between classification and the multisource reference data product. PA refers to the probability that ground-truth reference data for a category is correctly categorized. UA represents the probability that the validation point that falls into a category on the classification map is correctly classified into that category (Fan et al., 2015).

$$\text{OA} = \sum_{i=1}^n X_{ii} / N \quad (6)$$

$$\text{Kappa} = \frac{N \sum_{i=1}^n X_{ii} - \sum_{i=1}^n (X_{i+} \times X_{+i})}{N^2 - \sum_{i=1}^n (X_{i+} \times X_{+i})} \quad (7)$$

$$\text{PA}_i = X_{ii} / X_{i+} \quad (8)$$

$$\text{UA}_i = X_{ii} / X_{+i} \quad (9)$$

where  $n$  denotes the category,  $N$  represents the total number of samples,  $X_{ii}$  represents the number of diagonal elements of the confusion matrix,  $X_{i+}$  represents the sum of the columns of the category, and  $X_{+i}$  represents the sum of the rows of the category.

#### 2.3.4. Gravity-center migration model

The gravity center of desertification represents the point in the spatial plane at which torques balance for a specific desertification degree in a given year within the study area. The gravity center migration model comprehensively analyzes the direction, path, and distance of the gravity-center movement over a defined period, providing a clear and comprehensive depiction of desertification's spatial change characteristics (Na et al., 2019). The calculation formula is as follows:

$$X_t = \frac{\sum_{i=1}^n (C_{ti} \times X_i)}{\sum_{i=1}^n C_{ti}} \quad (10)$$

$$Y_t = \frac{\sum_{i=1}^n (C_{ti} \times Y_i)}{\sum_{i=1}^n C_{ti}} \quad (11)$$

where  $X_t$  and  $Y_t$  are the longitude and latitude coordinates of the center of gravity of the  $t^{\text{th}}$  desertification type, respectively;  $C_{ti}$  is the area of the  $i^{\text{th}}$  patch of the  $t^{\text{th}}$  degree of desertification; and  $X_i$  and  $Y_i$  are the longitude and latitude coordinates of the center of gravity of the  $i^{\text{th}}$  patch, respectively.

### 2.3.5. Geodetector

Geodetector is a statistical model used to detect the spatial heterogeneity of geographic phenomena and quantitatively reveal the drivers that affect their divergence. The model includes four components: factor, risk, ecological, and interaction detector (Wang and Xu, 2017). In this study, we selected 12 influencing factors (PRE, TMMN, TMMX, PET, VPD, SM, WS, PDSI, DEM, LU, POP, and LIVEST) from natural and social aspects. The effects of these factors on the spatial distribution and evolution of desertification in the MP, as well as the interactions between them, were then quantitatively identified using the factor detector and the interaction detector.

A factor detector can quantitatively detect the influence of factor  $X$  on the spatial differentiation of  $Y$ . In this study,  $X$  represents the 11 influencing factors, and  $Y$  is the desertification degree. The model is expressed as follows:

$$q = 1 - \frac{1}{N\sigma^2} \sum_{h=1}^L N_h \sigma_h^2 \quad (12)$$

where  $q$  is the explanatory or determining power of the impact factor on desertification in the MP, ranging from 0 to 1. A higher  $q$  value signifies increased influence of the factor on desertification and stronger explanatory power, whereas a lower value indicates diminished explanatory power.  $N$  is the number of samples in the study area;  $N_h$  is the number of samples with desertification degree ( $h$ );  $\sigma^2$  and  $\sigma_h^2$  are the variance of desertification in the study area and category  $h$ , respectively; and  $L$  is the number of desertification types.

Interaction detectors can determine whether the effects of factor interactions on desertification have been enhanced or weakened. There are five scenarios for the results of the interaction:  $P(X_1 \cap X_2) = P(X_1) + P(X_2)$ , for factors independent of each other;  $P(X_1 \cap X_2) < \min(P(X_1), P(X_2))$ , for nonlinear weakening;  $\min(P(X_1), P(X_2)) < P(X_1 \cap X_2) < \max(P(X_1), P(X_2))$ , for single factor nonlinearity weakening;  $P(X_1 \cap X_2) > P(X_1) + P(X_2)$ , denotes nonlinear enhancement; and  $P(X_1 \cap X_2) > \max(P(X_1), P(X_2))$  denotes bilinear enhancement.

## 3. Results

### 3.1. Potential occurrence range of desertification in the MP

Based on the MI, the potential extent of desertification on the MP is illustrated in Fig. 3. The potential occurrence area of desertification accounted for 83.88 % of the total land area, with the semi-arid zone

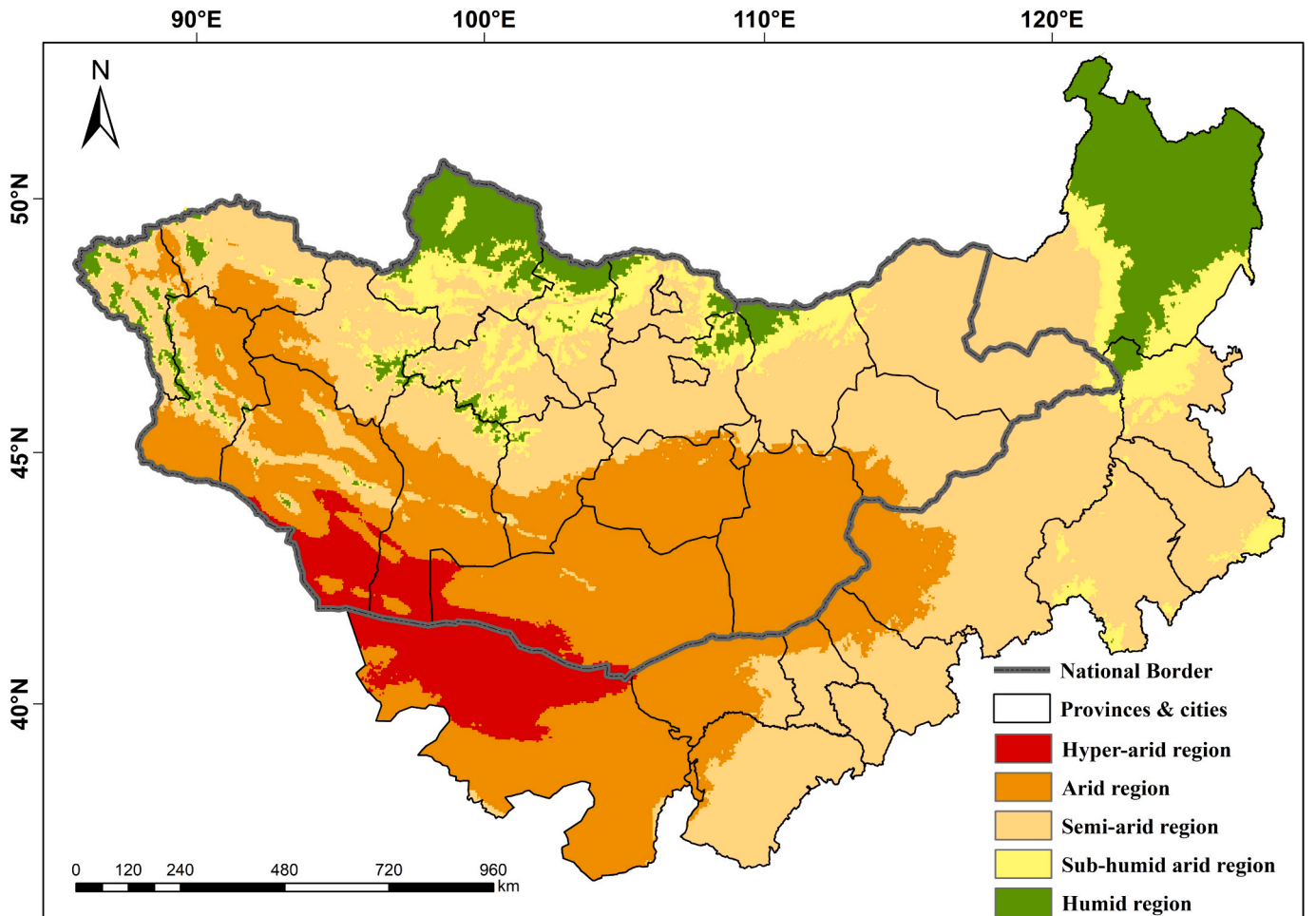


Fig. 3. Climate zoning map of the Mongolian Plateau.



constituting the largest portion at 44.03 %, followed by the arid zone. Non-desertification zones are primarily situated in the extremely arid and humid regions. The humid zone is mainly located in the Daxing'anling forest area in northeastern Inner Mongolia and in the Selenge River Basin in northern Mongolia.

3.2. Accuracy validation of desertification information extraction model

Fig. 4 illustrates the practical effects of different machine learning and feature space models for identifying desertification in the MP. The GBDT model exhibited superior performance in extracting each level of desertification. The revisions enhanced clarity and precision. The RF and SVM models performed as well as the GBDT model in recognizing light, moderate and heavy desertification. However, both were prone to misclassify potential desertified land and severe desertification as light and heavy desertification, respectively. The CART model is slightly better than the SVM model. The MMD model is ineffective in

distinguishing between potential desertification and moderate desertification, and misclassifies most of the potential desertification as light desertified land, but shows excellent performance in recognizing heavy and severe desertification. The Albedo -NDVI model is ineffective in distinguishing between potential, light, and moderate desertified land.

Table 4 shows the accuracy of different machine learning and feature space models in recognizing each desertification. The GBDT model had the highest accuracy with an overall accuracy of 88.18 % and a kappa coefficient of 0.85. Both its user accuracy and producer accuracy for identifying various desertification degrees were > 80 %, indicating its effectiveness in identifying different levels of desertified land. The overall accuracy of the RF model is high at 82.73 %, but the Kappa coefficient is relatively low at 0.71. The producer accuracies of the SVM and CART model for identifying severely desertified land were 21.43 % and 18.57 %, respectively, which were considerably lower than those for identifying other desertification degree. The producer accuracy of the MMD model for recognizing potential desertification was only 7.14 %,

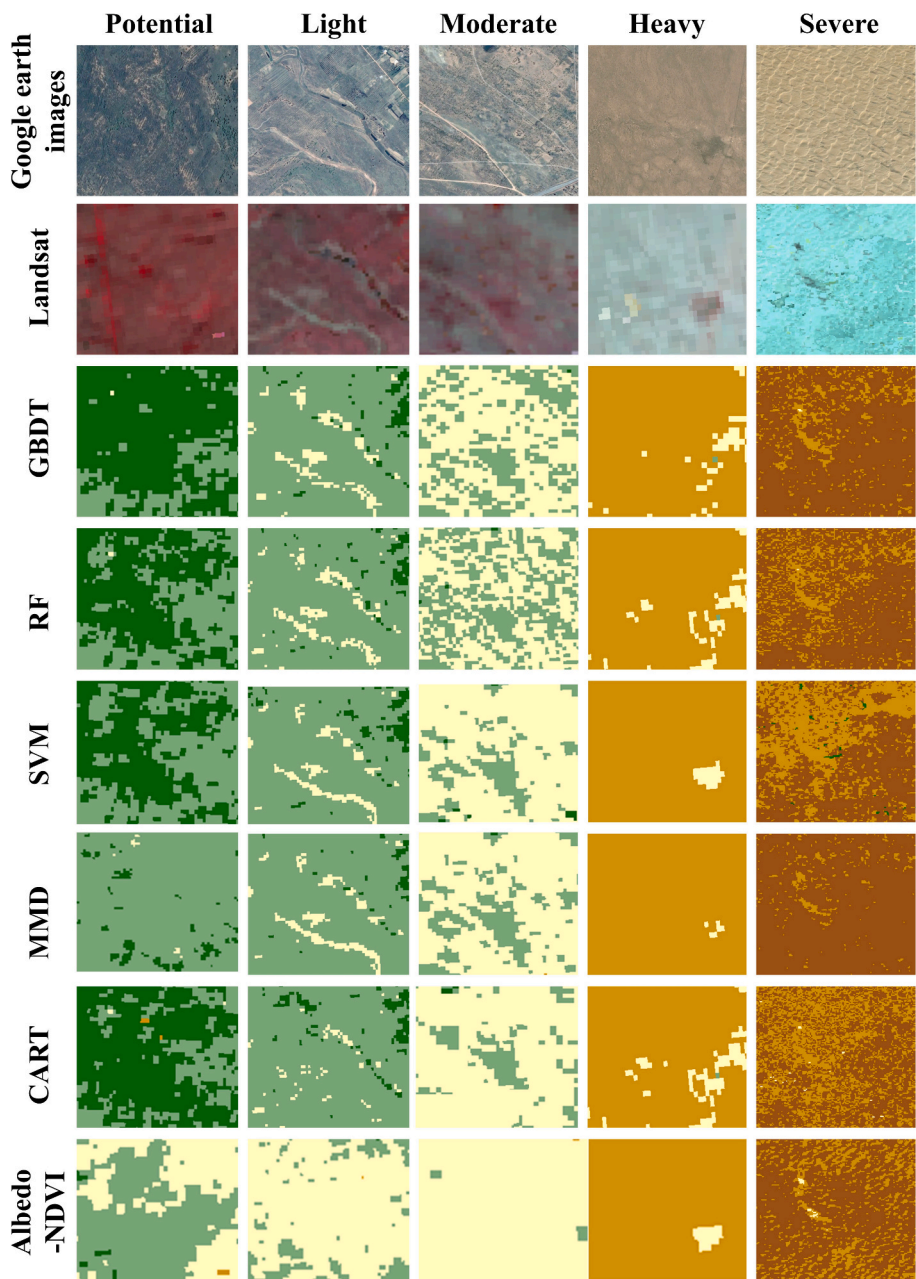


Fig. 4. Comparison of results from different desertification information extraction models.

**Table 4**  
Comparison of accuracy assessment of different desertification information extraction models.

Model	Potential		Light		Moderate		Heavy		Severe		OA (%)	Kappa
	PA (%)	UA (%)	PA (%)	UA (%)	PA (%)	UA (%)	PA (%)	UA (%)	PA (%)	UA (%)		
RF	82.14	85.19	82.14	79.31	86.36	90.47	94.44	70.83	64.29	100.0	82.73	0.71
GBDT	92.85	86.67	82.14	88.46	86.96	95.24	94.12	80.00	85.71	92.31	88.18	0.85
SVM	67.86	95.00	92.86	68.42	68.18	88.24	94.44	53.13	21.43	100.0	72.73	0.61
MMD	7.14	66.67	96.43	45.76	60.87	82.35	77.1	76.47	92.85	81.25	61.82	0.43
CART	71.42	100.0	85.71	72.73	82.61	76.00	82.35	51.85	28.57	80.00	73.64	0.66
Albedo-NDVI	3.57	100.0	10.71	13.04	100.0	36.51	40.06	88.89	92.85	92.85	43.64	0.22

indicating that most of the potentially desertified land was misclassified as other types. The user accuracies of the five machine learning models in recognizing different desertification levels were all above 45 %. The Albedo-NDVI feature space model recorded the lowest overall accuracy of 43.64 %. Therefore, compared with other models, the GBDT model is most suitable for extracting refined information on desertification in the Mongolian Plateau.

3.3. Spatial temporal pattern of desertification on the MP

Based on the gradient-boosting tree model, the degree of desertification in the MP was assessed from 1990 to 2020. In the last 30 years, potential and moderate desertification has been mainly concentrated in the northern and eastern regions of the MP, including the provinces of Khentii, Oriental, Sukhbaatar, Central, Bulgan, and Houhangai in northern Mongolia, and the cities of Hulunbeier, Xing'anmeng, and Tongliao in Inner Mongolia, China. Heavy and severe desertification was mainly found in the southwestern part of the MP including the South Gobi, East Gobi, Central Gobi, and former Hangai provinces in central and southern Mongolia and the Bayannur, Alashan, Baotou, and Ulan-qab cities in northern Inner Mongolia, China. Moderate desertification was mainly located within the transition zone between light and heavy desertification. From 1990 to 2000, potential and light desertification retreated to the north, while moderate and severe desertification experienced significant expansion in the same direction. From 2000 to 2005, severe desertification extended deeper into the hinterland of the MP. From 2005 to 2015, substantial areas of severe desertification reverted to heavy desertification, and moderately desertified land in the northern and eastern regions of the MP gradually shifted to potential or light desertification. While the area of potentially and lightly desertified land in northern Mongolia and southeastern Inner Mongolia further expanded from 2015 to 2020, the area of severely desertified land in southeastern Mongolia also expanded (Fig. 5).

From 1990 to 2020, the areas of potential, moderate, and severe desertification on the MP remained stable, accounting for approximately 19 %, 15 %, and 17 % of the total land area, respectively. The area of light desertification increased from 11.87 % to 16.27 %, and the area of severe desertification decreased from 14.64 % to 11.19 %. In 2000, the area of heavy desertification reached the largest in the last 30 years at 548,000 km<sup>2</sup>, accounting for 21.90 % of the total land area of the MP. The area of severe desertification reached its largest extent, with nearly 628,000 km<sup>2</sup> in 2005, accounting for 22.91 % of the total land area. The areas with different degrees of desertification in Inner Mongolia, China, and Mongolia were counted separately. From 1990 to 2020, the proportion of potentially desertified land in Inner Mongolia, China to its total area increased by 2.68 %, light desertification increased by 3.83 %, heavy desertification decreased by 2.23 %, and severe desertification decreased by 4.8 %. Since 2005, areas of both severe and heavy desertification in Inner Mongolia have continued to decline. From 1990 to 2020, the proportion of potentially desertified land in Mongolia to the total land area decreased by 2.60 %, light desertification increased by 4.83 %, and severe desertification decreased by 2.43 %. However, from 2015 to 2020, the area of severely desertified land in Mongolia increased

by 3.08 % (Fig. S2).

Fig. 6 illustrates the migration of the gravity centers for various degrees of desertification in the MP from 1990 to 2020. The gravity centers for potential and light desertification were closely situated, and their migration directions remained consistent. The movement of their gravity centers can be divided into two main periods: contraction, primarily towards the northwest and northeast from 1990 to 2010, and expansion towards the southwest and southeast from 2010 to 2020. Moderate desertification was mainly located within the transitional zone between heavy and light desertification, with shorter migration distances during all periods. Heavy desertification occurred over a maximum distance of 165 km. The movement of moderate, heavy, and severe desertification has a certain similarity, moving primarily northward from 1990 to 2005 and gradually shifting southward from 2005 to 2015. From 2015 to 2020, the center of moderate desertification continued to migrate southward, heavy desertification exhibited minimal northward movement, and severe desertification shifted westward.

3.4. Spatiotemporal evolution of desertification on the MP

The evolution of desertification on the MP from 1990 to 2020 was classified into five levels: significant deterioration (desertification intensifies by two or more levels), deterioration (desertification intensifies to the adjacent level), stabilization (desertification degree remains unchanged), recovery (desertification reduces to the adjacent level), and significant recovery (desertification is reduced by two or more levels). The dynamics of desertification on the MP from 1990 to 2020 can be divided into two periods: 1990–2010, marked by deterioration dominance, and 2010–2020, characterized by recovery dominance. Regions exhibiting highly active desertification conversion are concentrated in the Kent, Sukhbaatar, and Eastern provinces of northeastern Mongolia, as well as in the Xilingol League and Tongliao City in Inner Mongolia, China. Ongoing desertification has persisted over 30 years in the Omnogovi, Dornogovi, Dundgovi, and Bayankhongor provinces of Mongolia (Fig. 7). In the most severe period of land degradation on the Mongolian Plateau, from 1995 to 2000, the area experiencing deterioration and significant deterioration reached its peak, constituting approximately 18.79 % of the total land area. From 2010 to 2020, desertified land continued to deteriorate in the southwestern and southern regions of Mongolia, whereas Inner Mongolia, China achieved full recovery. From 2010 to 2015, the area of land recovery on the MP accounted for 26.8 % of the total area, which was approximately 1.5 times the area of deterioration. In the MP, Inner Mongolia, China, and Mongolia, the primary mode of deterioration involved transitions from moderate to severe desertification, and from heavy to severe desertification. In addition, the transition from potential to moderate desertification was the main mode of significant deterioration. The main modes of recovery involved transitions from severe to heavy desertification, heavy to moderate desertification, and moderate to light desertification (Fig. S3).



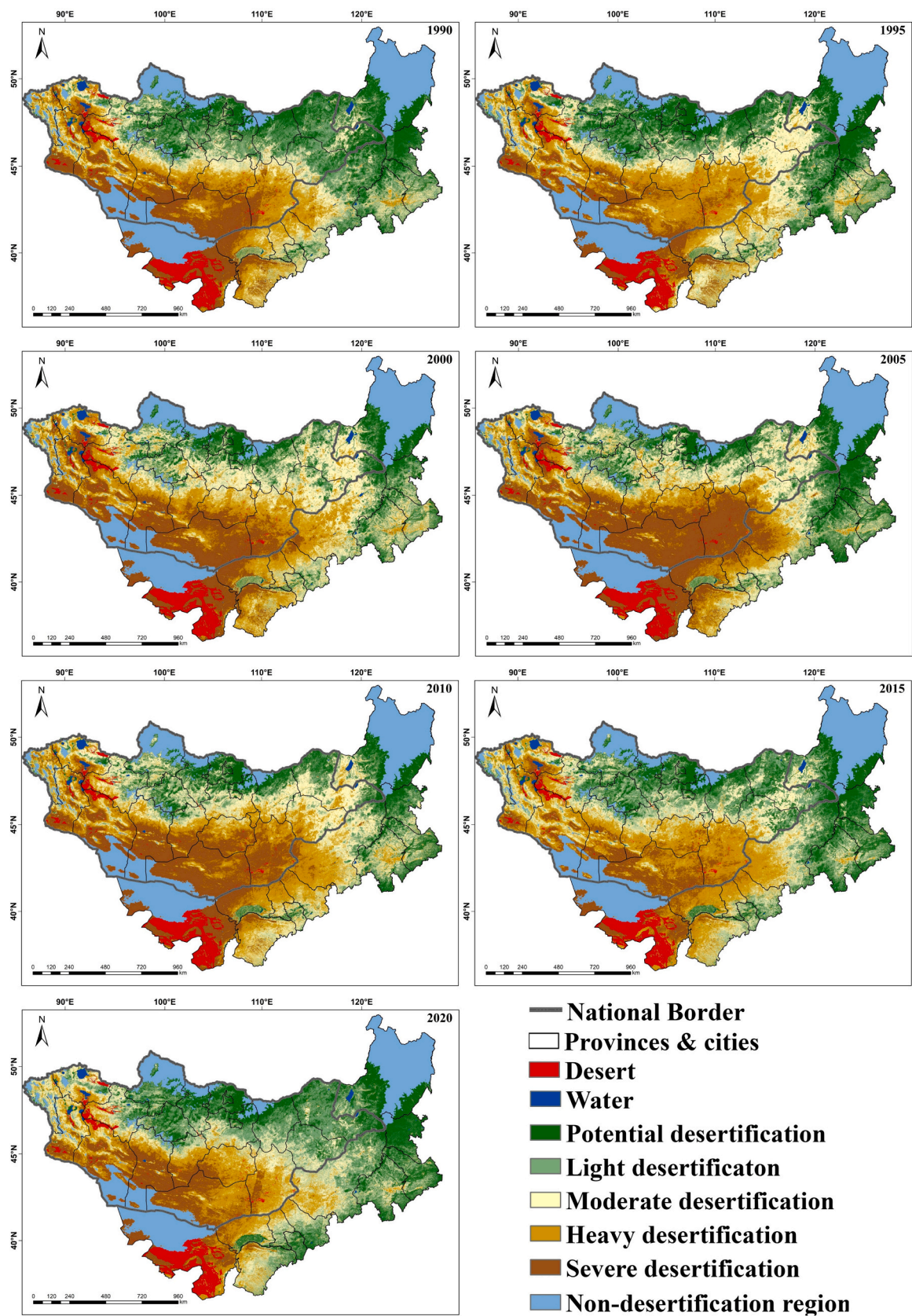


Fig. 5. The distribution of desertification degree in the MP from 1990 to 2020.



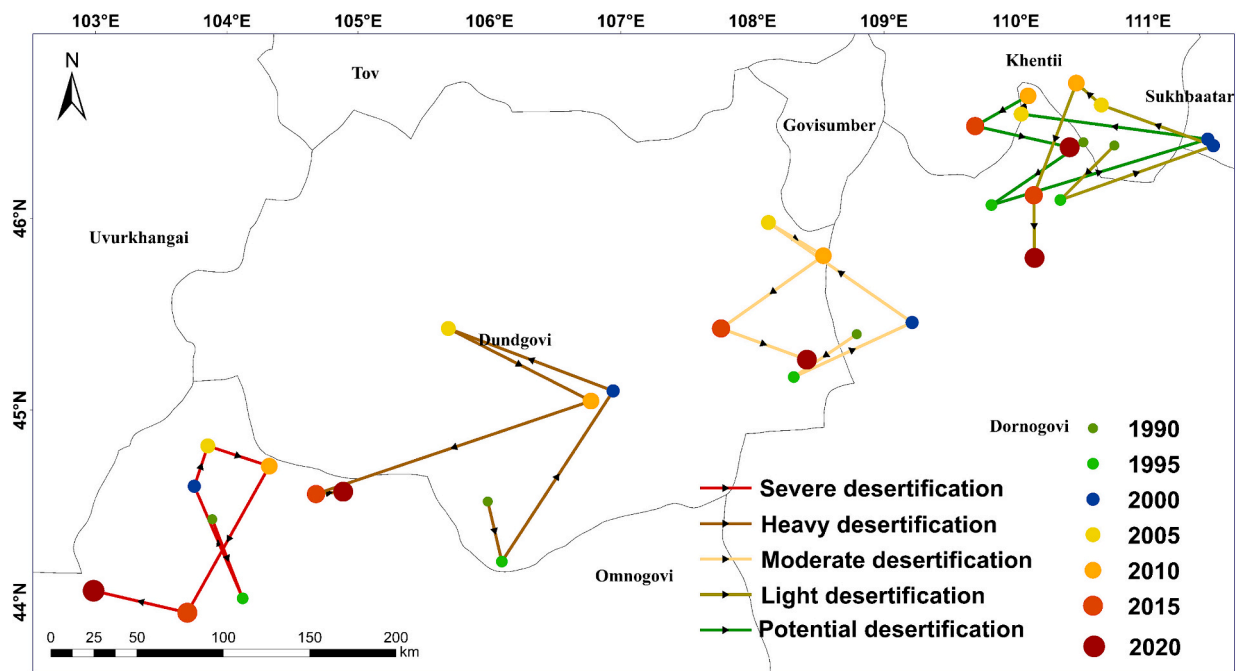


Fig. 6. Migration of the gravity center of desertification in the MP from 1990 to 2020.

### 3.5. Driving factors of desertification on the MP

#### 3.5.1. Driving factors of the spatial distribution of desertification

A total of 12 natural and anthropogenic factors, including POP, LIVEST, PDSI, PET, PRE, SM, TMMN, TMMX, VPD, WS, DEM, and LU, were selected to analyze the mechanism of driving spatial distribution patterns of desertification on the MP, Inner Mongolia, China, and Mongolia. The results of the one-factor detector revealed that, for the MP, PRE and LU were the dominant drivers. From 1990 to 2020, the  $q$ -value for PRE increases significantly, from 0.52 to 0.68. The  $q$ -value for LU remains stable between 0.4 and 0.5. The  $q$ -values for SM, WS, PET, TMMX and TMMN played secondary roles. However, the  $q$ -values for SM, WS, and PET decreased significantly. Conversely, the  $q$ -values for the remaining factors were  $< 0.2$ , suggesting negligible effects. Combining the results of the interaction model on the Mongolian Plateau, the  $q$ -values of the factor interactions were all significantly higher than those of the single factors, showing a nonlinear enhancement and bilinear enhancement relationship, and there were significant differences in the interactions between the different factors.  $PRE \cap (PET, TMMX, TMMN, \text{ and } LU)$  had the highest explanatory power, in the form of bilinear enhancement. PRE, SM, WS, and LU interacted with other factors in a predominantly bilinear enhancement form. The nonlinear enhancement was prevalent among PET, PDSI, TMMX, TMMN, VPD, LIVEST and DEM, indicating that the factor interactions would greatly enhance the explanatory power of these factors for the spatial distribution of desertification on the MP. For example, the Palmer Drought Index had a  $q$ -value of 0.07 in 2010, but the minimum  $q$ -value for the interaction with the other factors was 0.30 (Fig. 8).

In Inner Mongolia, China, PET and PRE were the predominant influences on the spatial distribution of desertification. The PET had the highest  $q$ -value of 0.65. Other factors also exerted a substantial influence. PRE and LU were the dominant drivers of the spatial distribution of desertification in Mongolia, and the  $q$ -values of PET, SM, TMMN, TMMX, and WS ranged from 0.32 to 0.45, significantly influencing the spatial distribution pattern of desertification. According to the results of factor interactions on the Inner Mongolia, China, and Mongolia, all interaction results belonged to the two categories of bilinear and nonlinear enhancement. In Inner Mongolia, China, the explanatory power of the interaction results of PRE and PET with other factors was

generally high, further verifying the dominant influence of both on the spatial differentiation of desertification; The nonlinear enhancement was prevalent among PDSI, TMMX, TMMN, VPD, LIVEST and POP. In Mongolia, the explanatory power of  $PRE \cap LU$  was the highest in all five years, with  $q$ -values of 0.71, 0.72, 0.75, 0.68, and 0.78, respectively. Meanwhile, the explanatory power of the interactions of PRE and LU with other factors was generally higher than the interaction results among other factors. Thus, it can be observed that the effects of natural and anthropogenic factors on the spatial distribution of desertification at different regional scales on the MP are not independent or simply stacked, but are the result of the interaction of multiple factors (Fig. S4-S5).

#### 3.5.2. Driving factors of desertification evolution

The changing rates of these natural and anthropogenic factors were obtained using slope trend analysis to further reveal the driving mechanisms of desertification evolution on the MP, Inner Mongolia, China, and Mongolia. In the MP, changes in LU exhibited the highest  $q$  values within the four phases of 2000–2020 ( $q = 0.5, 0.53, 0.48, \text{ and } 0.54$ ), establishing it as the primary driver on desertification evolution. The  $q$ -value of TMMN, WS, SM, and TMMX also influence desertification evolution, ranging from 0.2 to 0.4. Combining the results of the interaction model on the MP, the differences in the explanatory power of the interactions between LU and each of the other factors over the four periods in 2000–2020 are small, mainly in the form of bilinear enhancements; however, all are significantly higher than the effects of the interactions among the other factors. This further validates the dominant role of LU change in the evolution of desertification in the MP. The explanatory power of LIVEST and POP was low for individual factors, but was significantly enhanced by interactions with other climate factors. For example, in 2015–2020, the  $q$ -value of single-factor monitoring of LIVEST was 0.14, which was significantly enhanced by interaction with PRE, TMMX, and TMMN, resulting in  $q$ -values of 0.47, 0.53, and 0.48, respectively. With the exception of LU, WS and SM, the interaction results for the other factors predominantly exhibited as nonlinear enhancements (Fig. 9).

In Inner Mongolia, the explanatory power of single factors for desertification evolution are relatively low. In 2000–2005, the order of the top five factors in terms of explanatory power, from high to low, was

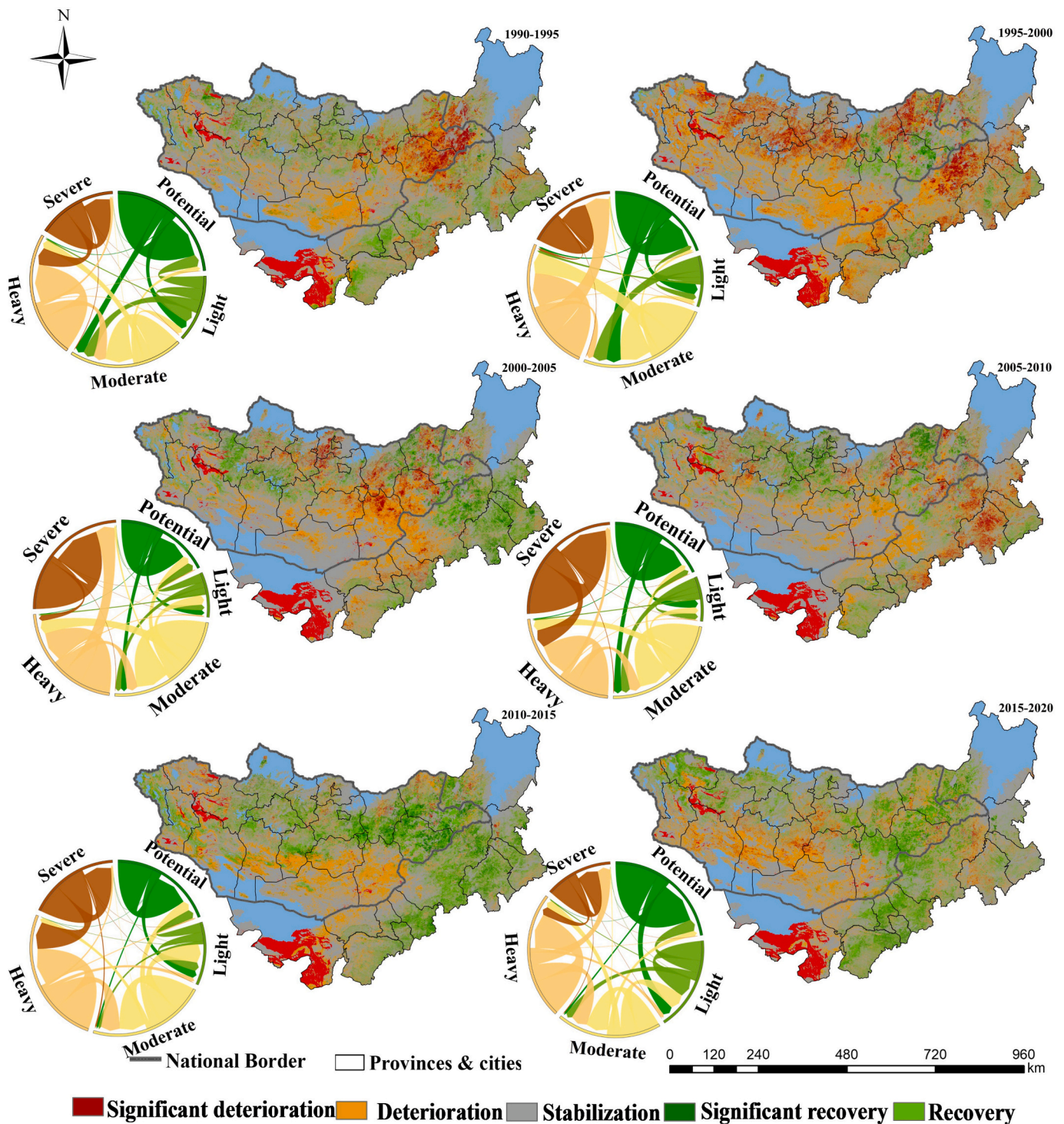


Fig. 7. Spatial distribution of desertification conversion on the Mongolian Plateau from 1990 to 2020.

TMMN ( $q = 0.45$ ) > SM ( $q = 0.42$ ) > WS ( $q = 0.41$ ) > LIVEST ( $q = 0.34$ ) > PRE ( $q = 0.3$ ). In 2005–2010, the order was TMMN ( $q = 0.34$ ) = LU ( $q = 0.34$ ) > TMMX ( $q = 0.29$ ) > LIVEST ( $q = 0.28$ ) > POP ( $q = 0.27$ ). In 2010–2015, the order was LIVEST ( $q = 0.38$ ) > VPD ( $q = 0.35$ ) > LU ( $q = 0.29$ ) > WS ( $q = 0.27$ ) = SM ( $q = 0.27$ ). In 2015–2020, the order was TMMX ( $q = 0.43$ ) > TMMN ( $q = 0.41$ ) > LU ( $q = 0.35$ ) > LIVEST ( $q = 0.33$ ) > VPD ( $q = 0.29$ ). A single factor does not explain well the evolution of desertification in Inner Mongolia, China. However, nonlinear enhancement and bilinear enhancement approaches are prevalent in factors such as TMMX, TMMN, LU, and LIVEST, indicating that the

desertification evolution in Inner Mongolia is mainly influenced by the combined effects of LIVEST, TMMX, TMMN, LU, and other factors. In Mongolia, the  $q$ -value of LU change is the highest and significantly greater than that of other factors. Thus, LU emerges as the dominant driver of desertification evolution. Meanwhile, the explanatory power of the interaction between LU and each of the other factors (average  $q$ -value > 0.70) were all significantly higher than the effects of the interactions among the other factors. With the exception of LU, the interaction results for the other factors predominantly performed as nonlinear enhancements (Fig. S6-S7).



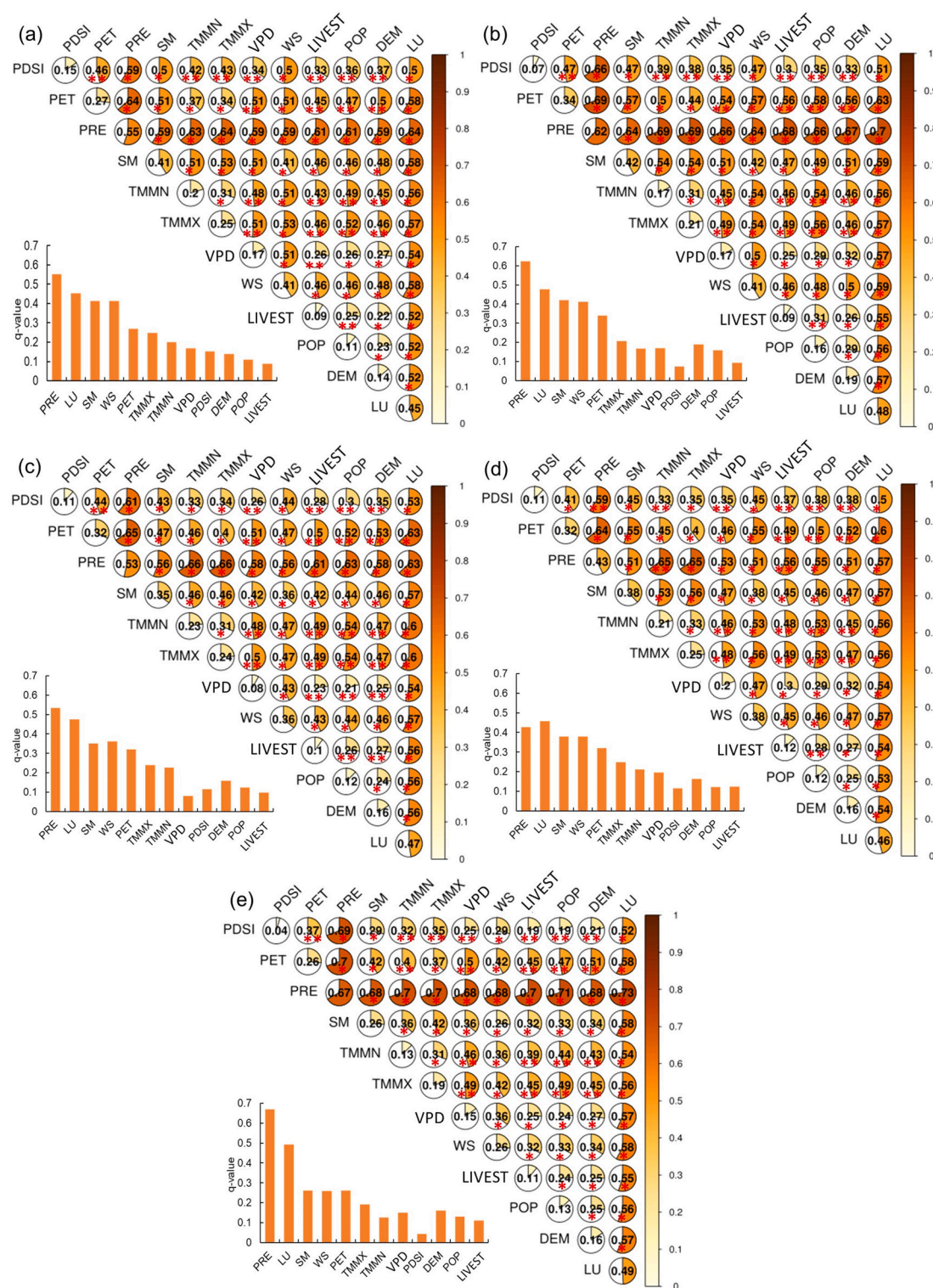


Fig. 8. Explanatory power of factors on the spatial distribution pattern of desertification in MP. (a)2000 (b)2005 (c)2010 (d)2015 (e)2020.

## 4. Discussion

### 4.1. Large-scale and high-refined desertification information extraction program

As the largest arid and semi-arid region in the northern hemisphere, desertification is a major ecological and environmental challenge in the MP. For a large-scale region with complex geography, many studies tend

to ignore the identification on the potential extent of desertification occurrence (Fan et al., 2020; Meng et al., 2021; Guo et al., 2022; Ren et al., 2024), resulting in a broad classification of desertification degree across the entire study area, which reduces the scientific and accuracy of data production and analysis. In this study, we utilized meteorological data to recognize the potential extent of desertification occurrence on the MP based on the humidity index.

Vegetation growth status is a key indicator for remote sensing



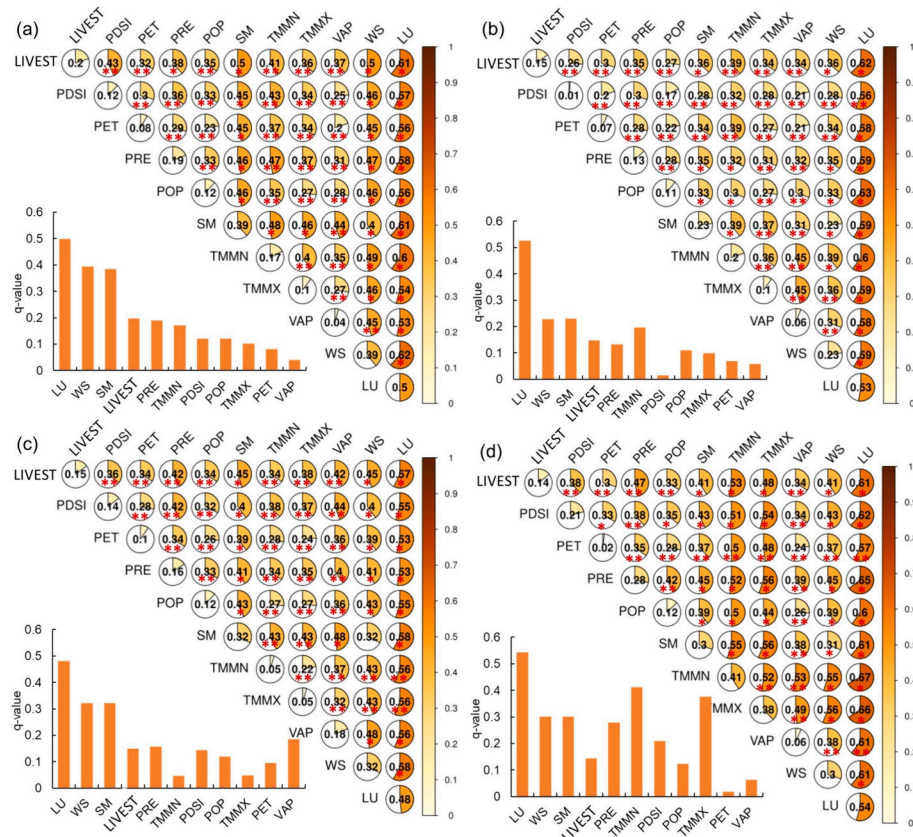


Fig. 9. Explanatory power of factors on the evolution of desertification in MP. (a)2000–2005 (b)2005–2010 (c)2010–2015(d)2015–2020.

evaluation of desertification. However, in arid and semi-arid areas, the surface vegetation is sparse, the vegetation signal is weak, and the sensitivity of vegetation growth to precipitation is high. Therefore, compared with methods that use the median surface reflectance of all effective pixels during the growing season to synthesize the whole-area image (Meng et al., 2021), the NDVI maximum synthesis method adopted in this study can sensitively capture more effective vegetation information during the limited growing season, improve the accuracy of vegetation monitoring, and further enhance the distinction between sparsely vegetated areas and bare land. Vegetation indicators and soil indicators based on remote sensing inversion are indispensable in desertification monitoring. Desertification thematic characteristics, such as FCV, NDVI, MSAVI, Albedo, and TGSI, are commonly used to train machine learning models for desertification inversion. However, spectral information, which is a fundamental feature of remote sensing classification, is often overlooked in desertification identification (Fan et al., 2020; Feng et al., 2022; Zhao et al., 2023). Consequently, in utilizing thematic indicators for desertification assessment, we fully considered the six spectral features (green, blue, red, near-infrared, short-wave infrared 1, and short-wave infrared 2) of the Landsat image for model training. This approach identifies detailed features with different levels of desertification thus avoiding significant polarization of the recognition accuracy for different desertification degrees.

In this study, using the GEE platform, we compared the performances of five machine learning methods and the Albedo-NDVI feature space model for large-scale and high-fine desertification information extraction. Among these, the gradient-boosted tree algorithm exhibited the highest overall accuracy and Kappa coefficient, indicating its effectiveness in recognizing the overall desertification in the Mongolian Plateau and its balanced performance in recognizing each desertification level. The random forest model exhibited a better effect in recognizing the overall desertification, but its Kappa coefficient was lower than that of

the gradient boosted tree method. The other machine learning models exhibited low overall accuracy and evident performance gaps in recognizing different desertification levels. Due to its consideration of the relationship between two indicators only, the single-feature space model has poor recognition accuracy and cannot be applied to the recognition of large-scale desertification information with complex geographic conditions.

The MP has a complex geographic environment with obvious geographic heterogeneity, and a single machine learning model has high result uncertainty in different interior geographic units. In addition, due to the lack of high spatial and temporal resolution data on soil attributes, such as soil organic carbon, and climate data in the MP, utilizing a few vegetation and soil indicators obtained by inversion of remote sensing images can reduce, but not completely avoid, the impact of long-term climate fluctuations on the extraction of refined desertification information and the succession process in the region, especially in the transition between arid and semi-arid areas (Wessels et al., 2004). Therefore, future research should focus on the combination of different geographic units and machine learning models, and further explore remote sensing inversion indicators that can reflect soil attributes and climate characteristics, as well as soil attributes and climate products with high spatial and temporal resolution.

#### 4.2. Differences in the evolution of desertification in Mongolia and Inner Mongolia, China

China's Inner Mongolia is adjacent to Mongolia and has similar geographical and environmental conditions. Between 1990 and 2005, desertification deteriorated in both Mongolia and Inner Mongolia, China, which is consistent with the results of previous studies (Liu et al., 2020; Meng et al., 2021). Post-2005, distinctions emerged in the evolution of desertification between Inner Mongolia, China, and Mongolia.

Between 2005 and 2010, Inner Mongolia experienced persistent land degradation, transitioning from potential light desertification to moderate desertification. From 2010 to 2020, desertified land in Inner Mongolia, China, entered a state of full recovery. However, desertification in Mongolia rapidly deteriorated from 2015 to 2020, following a slight reversal from 2005 to 2015. Overall, in the past 30 years, the degree of desertification in Inner Mongolia has improved, while that in Mongolia has increased.

The improvement and deterioration of desertified land depends on climate change and the intensity of human activities. Since the 1980s, the annual average temperature in Mongolia has risen by approximately 1.5 °C–2.5 °C, which is two to four times the global average rise level (Wang et al., 2020; Liang et al., 2021). The significant increase in temperature may exacerbate the drought and the frequency of heat waves (Hirschi et al., 2011), leading to further deterioration of desertified land. During the period of 1990–2020, the overall decreasing trend of precipitation in Mongolia is divided into two main phases: in 1990–2005, the decreasing trend of precipitation is unfavorable for vegetation growth; and in 2005–2020, the increasing trend of precipitation promotes the growth of vegetation. Overgrazing has further aggravated the deterioration of desertified land in Mongolia. Since the early 1990s, Mongolia has been implementing a planned economy and a husbandry policy whereby “pastureland is owned by herders” and “livestock is privately owned” (Saizen et al., 2010). To earn the right to use pastureland and to pursue economic benefits, the herder sector has competed to increase the number of livestock and raise large numbers of goats. From 1990 to 2020, the total number of livestock increased by approximately 41.75 million heads, or 1.6 times; the total number of goats increased by approximately 22.6 million head, or 4.41 times. The sharp increase in the total number of livestock and the imbalance in the livestock structure have exacerbated grassland degradation and land desertification. In response to desertification, Mongolia has also formulated a series of laws and regulations and ecological restoration projects, including the National Program on Combating Desertification and the National “Green Wall” Program. Although these measures are expected to play a key role in preventing desertification, they have had little effect due to limited funding and lack of continuity (Liang et al., 2021). In contrast to climate change and human activities in Mongolia, there was an overall increasing trend in precipitation in Inner Mongolia, China, during the 1990–2020 period, which was divided into three main phases: an increasing trend in precipitation from 1990 to 2000, a decreasing trend from 2000 to 2010, and an increasing trend from 2010 to 2020. Meanwhile, the intensity of grazing in Inner Mongolia, China, has increased, with livestock numbers increasing by 33.48 million head between 2000 and 2010, but remaining stable thereafter. However, differing from the nomadic grazing approach in Mongolia, Inner Mongolia has implemented a strict strategy of sealing and shifting of pastures by prohibiting grazing, resting pastures, rotating pastures, and foddering since the beginning of 2000. This strategy has promoted a fundamental change in livestock production and management modes, as well as a strategic adjustment of the economic structure, reducing the pressure on the utilization of grassland resources (Du et al., 2015).

Variances in the evolution of desertification between China and Mongolia, as two politically independent entities, are primarily shaped by their ecological restoration policies and engineering initiatives (Chan et al., 2023; Guo et al., 2021; Meng et al., 2021; Zhao et al., 2023). In 1978, China launched 16 ecological restoration projects with significant investments and far-reaching impacts. These projects, such as the “Three-North” protection forest system construction, Beijing-Tianjin wind and sand source management, natural forest protection, and the return of farmland to forests and grasslands, have substantially curtailed the expansion of desertification in China by enhancing ground cover and mitigating the spread of wind-blown sand (Bryan et al., 2018). Nevertheless, the Three-North Protective Forest Program and the Sand Control and Sand Management Program, implemented in the 1980s, exhibited delayed effects. The initial restorative effects of these programs have not

been sufficient to counterbalance the negative effects of socioeconomic development (Liu et al., 2020). Additionally, afforestation projects in arid and semi-arid areas intensify soil moisture depletion and increase the pressure on groundwater demand, posing challenges for the survival of planted trees and degradation of native grassland vegetation, thus adversely affecting the recovery of desertified land (Cao, 2011, 2008; Veldman et al., 2015). After analyzing the lessons learned from prior afforestation efforts, China shifted its focus to natural restoration and regional vegetation restructuring. It has also increased financial investment in projects like the protection of natural forests (Cao et al., 2011; Liu et al., 2020). Consequently, the effectiveness of the ecological restoration projects has significantly improved.

#### 4.3. Mechanisms driving the spatial distribution and evolution of desertification

Interactions between natural and anthropogenic factors can lead to desertification. Precipitation has been identified as a key factor influencing the distribution of desertification on the MP in Inner Mongolia, China, and Mongolia, consistent with existing results (Fan et al., 2020; Guo et al., 2021; Meng et al., 2021). In arid and semiarid regions, precipitation is a critical constraint affecting vegetation activity, and a lack of water tends to inhibit plant growth. Vegetation responds more to changes in precipitation than temperature, indicating that precipitation has a greater impact on vegetative dynamics (Herrmann et al., 2005; Pueyo et al., 2013; Zhu et al., 2019). As a result, the southern and northern parts of the MP, which receive ample precipitation, are primarily characterized by potential desertification and mild desertification. In contrast, the southern regions of Mongolia and the northern part of Inner Mongolia, China, which experience sparse precipitation, are predominantly characterized by heavy and severe desertification. In Inner Mongolia, China, potential evapotranspiration is an important driver of desertification. Potential evapotranspiration refers to the maximum rate of water evaporation under specific environmental conditions, including temperature, humidity, wind speed, and sufficient moisture. This parameter reflected the vegetative growth environment. Warm and dry environments are unfavorable for vegetation growth, making severe desertification more likely in areas with high potential evapotranspiration (Zhang et al., 2020). The distribution of precipitation in Inner Mongolia was generally consistent with the distribution of potential evapotranspiration.

Contrary to the spatial distribution pattern of desertification, the results of this study suggest that changes in land use are the primary factor influencing the evolution of desertification in this region. Fig. 10 illustrates the conversion of land use on the MP. The central part of the MP is a region of frequent land-use change and extremely active desertification conversion. Land use change can to some extent represent changes in the intensity of human activities, such as overgrazing that turns former grassland into bare land. Reforestation, grazing prohibition and rest grazing policies are considered to be the primary drivers of land reclamation (Wang et al., 2023a; Liu et al., 2020; Zhai et al., 2023). However, afforestation has been associated with reduced soil moisture and a lowering of the water table, as well as social impacts such as increased water shortages for populations and livestock in some cases, and resource enclosures that are particularly detrimental to the pastoralists livelihoods (Turner et al., 2023). Thus, the environmental and social impacts of a range of ecological restoration policies require monitoring in the medium and long term. Strong wind speeds can carry away soil nutrients and fine particles, leading to sand formation, further exacerbating land degradation (Chang et al., 2021; Huang et al., 2020). Previous research has indicated that the greening of drylands is primarily influenced by weakened wind speed and increased precipitation in spring, which is consistent with our findings (Li et al., 2021). Soil moisture reflects the amount of water available to vegetation more directly than changes in precipitation. The proliferation of livestock and population, increasing temperatures, and other natural factors can



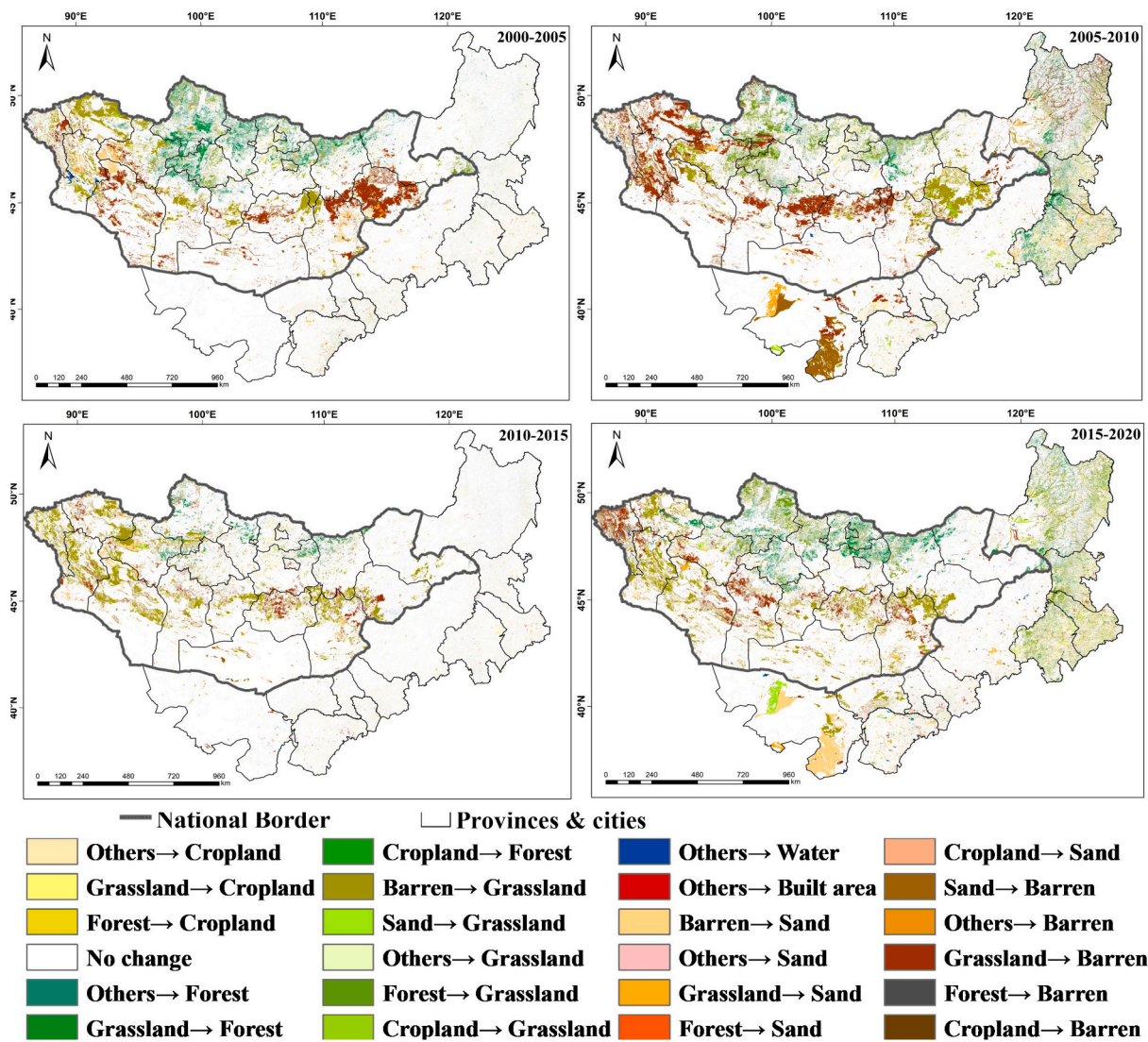


Fig. 10. Land use conversion on the MP from 1990 to 2020.

contribute to increased desertification to some extent (Chi et al., 2019; Meng et al., 2021). Consequently, factor interactions significantly enhanced the explanatory power of desertification evolution in various regions of the MP, surpassing that of a single factor. This suggests that the evolution of desertification was influenced by multiple factors, including changes in soil moisture, wind speed, and livestock.

5. Conclusions

In this study, the potential occurrence range of desertification on the Mongolian Plateau was initially determined. An indicator system and optimal machine learning model suitable for extracting refined desertification information on the MP were constructed based on the GEE platform. Furthermore, the distribution map of desertification degree on the entire MP from 1990 to 2020 was drawn using the optimal machine learning model. Finally, the spatial - temporal patterns and evolution of desertification in the MP were analyzed, and the dominant drivers of desertification distribution and evolution were further identified. The main conclusions are as follows:

- (1) The potential desertification range covered 83.88 % of the total land area, with non-desertification regions situated in the northern and southwestern parts of the MP.

- (2) The gradient boosted tree model exhibited the highest overall accuracy of 88.18 %, and kappa coefficient of 0.85. Both the user's accuracy and producer's accuracy of recognizing different degrees of desertification are relatively stable, making it suitable for fine monitoring of large-scale dryland desertification.
- (3) From 1990 to 2020, the proportion of light desertification increased by 4.40 %, the proportion of severe desertification decreased by 3.45 %, and the area of other desertification degrees remained stable. Heavy and severe desertification was mainly found in the southwestern part of the MP. The MP experienced predominant land degradation from 1990 to 2010, transitioning to land restoration from 2010 to 2020. In 2005, differences in desertification evolution emerged between Inner Mongolia, China, and Mongolia.
- (4) PRE and LU are the main drivers of the spatial distribution pattern of desertification in the MP and Mongolia. PET and PRE are the main influencing factors in Inner Mongolia. Variations in LU is the primary drivers of desertification on the MP in Inner Mongolia, China. The desertification evolution in Inner Mongolia is mainly affected by the interaction of LIVEST, TMMX, TMMN, and LU.

This study aims to enhance our understanding of the overall



desertification pattern, evolution, and driving mechanisms of the MP. It also explores the differences in desertification evolution and drivers among Inner Mongolia, China, and Mongolia. This study seeks to promote the realization of the LDN goal and foster in-depth cooperation between China and Mongolia for desertification control. However, in order to improve the problem of result uncertainty in different internal geographic units and the impact of long-term climate fluctuations on desertification evolution, the combination of different geographic units and machine learning algorithms requires further in-depth investigations, with the introduction of vegetation and soil indicators.

### CRedit authorship contribution statement

**Shuxing Xu:** Writing – review & editing, Writing – original draft, Visualization, Validation, Methodology, Investigation, Data curation, Conceptualization. **Juanle Wang:** Writing – review & editing, Supervision, Conceptualization. **Ochir Altansukh:** Writing – review & editing. **Togtokh Chuluun:** Writing – review & editing.

### Declaration of competing interest

The authors declare that they have no known competing financial interests or personal relationships that could have appeared to influence the work reported in this paper.

### Data availability

Data will be made available on request.

### Acknowledgments

This research was funded by the National Key R&D Program of China (2022YFE0119200), Project “32161143025” and “41971385” supported by NSFC, Science & Technology Fundamental Resources Investigation Program of China (2022FY101902), Key Project of Innovation LREIS (KPI006), Mongolian Foundation for Science and Technology (NSFC 2022/01, CHN2022/276) and National University of Mongolia (P2023-4429, P2022-4256).

### Appendix A. Supplementary data

Supplementary data to this article can be found online at <https://doi.org/10.1016/j.scitotenv.2024.173566>.

### References

- Abatzoglou, J., Dobrowski, S., Parks, S., Hegewisch, K., 2018. TerraClimate, a high-resolution global dataset of monthly climate and climatic water balance from 1958–2015. *Sci. Data* 5, 170191. <https://doi.org/10.1038/sdata.2017.191>.
- Alherbawi, M., McKay, G., Govindan, R., Haji, M., Al-Ansari, T., 2022. A novel approach on the delineation of a multipurpose energy-greenbelt to produce biofuel and combat desertification in arid regions. *J. Environ. Manag.* 323, 116223 <https://doi.org/10.1016/j.jenvman.2022.116223>.
- Bardgett, R.D., Bullock, J.M., Lavorel, S., Manning, P., Schaffner, U., Ostle, N., Chomel, M., Durigan, G.L., Fry, E., Johnson, D., Lavallee, J.M., Le Provost, G., Luo, S., Png, K., Sankaran, M., Hou, X., Zhou, H., Ma, L., Ren, W., Li, X., Ding, Y., Li, Y., Shi, H., 2021. Combating global grassland degradation. *Nat. Rev. Earth Environ.* 2, 720–735. <https://doi.org/10.1038/s43017-021-00207-2>.
- Belgiu, M., Drăguț, L., 2016. Random forest in remote sensing: a review of applications and future directions. *ISPRS J. Photogramm. Remote Sens.* 114, 24–31. <https://doi.org/10.1016/j.isprsjprs.2016.01.011>.
- Berdugo, M., Kéfi, S., Soliveres, S., Maestre, F., 2017. Plant spatial patterns identify alternative ecosystem multifunctionality states in global drylands. *Nat. Ecol. Evol.* 1, 1–10. <https://doi.org/10.1038/s41559-016-0003>.
- Bryan, B., Gao, L., Ye, Y., Sun, X., Connor, J., Crossman, N., Stafford-Smith, M., Wu, J., He, C., Yu, D., Liu, Z., Li, A., Huang, Q., Ren, H., Deng, X., Zheng, H., Niu, J., Han, G., Hou, X., 2018. China's response to a national land-system sustainability emergency. *Nature* 559, 193–204. <https://doi.org/10.1038/s41586-018-0280-2>.
- Cao, S., 2008. Why large-scale afforestation efforts in China have failed to solve the desertification problem. *Environ. Sci. Technol.* 42, 1826–1831. <https://doi.org/10.1021/es08070597>.
- Cao, S., 2011. Impact of China's large-scale ecological restoration program on the environment and Society in Arid and Semiarid Areas of China: achievements, problems, synthesis, and applications. *Crit. Rev. Environ. Sci. Technol.* 41, 317–335. <https://doi.org/10.1080/10643380902800034>.
- Cao, S., Chen, L., Shankman, D., Wang, C., Wang, X., Zhang, H., 2011. Excessive reliance on afforestation in China's arid and semi-arid regions: lessons in ecological restoration. *Earth Sci. Rev.* 104, 240–245. <https://doi.org/10.1016/j.earscirev.2010.11.002>.
- Chan, F.K.S., Chen, J., Li, P., Wang, J., Wang, J., Zhu, Y., 2023. The cross-boundary of land degradation in Mongolia and China and achieving its neutrality - challenges and opportunities. *Ecol. Indic.* 151, 110311 <https://doi.org/10.1016/j.ecolind.2023.110311>.
- Chang, X., Sun, L., Yu, X., Liu, Z., Jia, G., Wang, Y., Zhu, X., 2021. Windbreak efficiency in controlling wind erosion and particulate matter concentrations from farmlands. *Agric. Ecosyst. Environ.* 308, 107269 <https://doi.org/10.1016/j.agee.2020.107269>.
- Chi, W., Zhao, Y., Kuang, W., He, H., 2019. Impacts of anthropogenic land use/cover changes on soil wind erosion in China. *Sci. Total Environ.* 668, 204–215. <https://doi.org/10.1016/j.scitotenv.2019.03.015>.
- Christian, B.A., Dhinwa, P.S., Ajai, 2018. Long term monitoring and assessment of desertification processes using medium & high resolution satellite data. *Appl. Geogr.* 97, 10–24. <https://doi.org/10.1016/j.apgeog.2018.04.010>.
- Ding, H., Hao, M., 2021. Spatiotemporal change and drivers analysis of desertification in the arid region of Northwest China based on geographic detector. *Environ. Chall.* 4, 100082 <https://doi.org/10.1016/j.envc.2021.100082>.
- Du, F., Guimu, J., Dags, K., 2015. Grassland livestock husbandry in China and Mongolia comparative study of management. *World Forest.* 8, 157–161. <https://doi.org/10.13856/j.cn11-1097/s.2015.08.032>.
- Duan, H., Wang, T., Xue, X., Yan, C., 2019. Dynamic monitoring of aeolian desertification based on multiple indicators in Horqin Sandy Land, China. *Sci. Total Environ.* 650, 2374–2388. <https://doi.org/10.1016/j.scitotenv.2018.09.374>.
- Fan, Z., Li, J., Yue, T., Zhu, X., Lan, A., 2015. Scenarios of land cover in karst area of southwestern China. *Environ. Earth Sci.* 74, 6407–6420. <https://doi.org/10.1007/s12665-015-4223-z>.
- Fan, Z., Li, S., Fang, H., 2020. Explicitly identifying the desertification change in CMREC area based on multisource remote data. *Remote Sens.* 12, 3170. <https://doi.org/10.3390/rs12193170>.
- Feng, K., Wang, T., Liu, S., Kang, W., Chen, X., Guo, Z., Zhi, Y., 2022. Monitoring desertification using machine-learning techniques with multiple indicators derived from MODIS images in mu us Sandy land. *China. Remote Sens.* 14, 2663. <https://doi.org/10.3390/rs14112663>.
- Feng, Q., Ma, H., Jiang, X., Wang, X., Cao, S., 2015. What has caused desertification in China? *Sci. Rep.* 5, 15998. <https://doi.org/10.1038/srep15998>.
- Guo, B., Wei, C., Yu, Y., Liu, Y., Li, J., Meng, C., Cai, Y., 2022. The dominant influencing factors of desertification changes in the source region of Yellow River: climate change or human activity? *Sci. Total Environ.* 813, 152512 <https://doi.org/10.1016/j.scitotenv.2021.152512>.
- Guo, X., Chen, R., Thomas, D., Li, Q., Xia, Z., Pan, Z., 2021. Divergent processes and trends of desertification in Inner Mongolia and Mongolia. *Land Degrad. Dev.* 32, 3684–3697. <https://doi.org/10.1002/ldr.3825>.
- Herrmann, S., Anyamba, A., Tucker, C., 2005. Recent trends in vegetation dynamics in the African Sahel and their relationship to climate. *Glob. Environ. Chang.* 15, 394–404. <https://doi.org/10.1016/j.gloenvcha.2005.08.004>.
- Hirschi, M., Seneviratne, S., Alexandrov, V., Boberg, F., Boroneant, C., Christensen, O., 2011. Observational evidence for soil-moisture impact on hot extremes in southeastern Europe. *Nat. Geosci.* 4, 17–21. <https://doi.org/10.1038/ngeo1032>.
- Huang, J., Ma, J., Guan, X., Li, Y., He, Y., 2019. Progress in semi-arid climate change studies in China. *Adv. Atmos. Sci.* 36, 922–937. <https://doi.org/10.1007/s00376-018-8200-9>.
- Huang, J., Zhang, G., Zhang, Y., Guan, X., Wei, Y., Guo, R., 2020. Global desertification vulnerability to climate change and human activities. *Land Degrad. Dev.* 31, 1380–1391. <https://doi.org/10.1002/ldr.3556>.
- Huete, A.R., 1988. A soil-adjusted vegetation index (SAVI). *Remote Sens. Environ.* 25, 295–309. [https://doi.org/10.1016/0034-4257\(88\)90106-X](https://doi.org/10.1016/0034-4257(88)90106-X).
- IPCC, 2019. Climate Change and Land: An IPCC Special Report on Climate Change, Desertification, Land Degradation, Sustainable Land Management, Food Security, and Greenhouse Gas Fluxes in Terrestrial Ecosystems. Summary for Policymakers. <https://www.ipcc.ch/site/assets/uploads/2019/08/Fullreport-1.pdf>.
- Jiang, Z., Ni, X., Xing, M., 2023. A study on spatial and temporal dynamic changes of desertification in northern China from 2000 to 2020. *Remote Sens.* 15, 1368. <https://doi.org/10.3390/rs15051368>.
- Li, C., Fu, B., Wang, S., Stringer, L.C., Wang, Y., Li, Z., Liu, Y., Zhou, W., 2021. Drivers and impacts of changes in China's drylands. *Nat. Rev. Earth Environ.* 2, 858–873. <https://doi.org/10.1038/s43017-021-00226-z>.
- Li, N., Yan, C.Z., Xie, J.L., 2015. Remote sensing monitoring recent rapid increase of coal mining activity of an important energy base in northern China, a case study of mu us Sandy land. *Resour. Conserv. Recycl.* 94, 129–135. <https://doi.org/10.1016/j.resconrec.2014.11.010>.
- Li, Q., Zhang, C., Shen, Y., Jia, W., Li, J., 2016. Quantitative assessment of the relative roles of climate change and human activities in desertification processes on the Qinghai-Tibet plateau based on net primary productivity. *CATENA* 147, 789–796. <https://doi.org/10.1016/j.catena.2016.09.005>.
- Li, W., Dong, R., Fu, H., Wang, J., Yu, L., Gong, P., 2020. Integrating Google earth imagery with Landsat data to improve 30-m resolution land cover mapping. *Remote Sens. Environ.* 237, 111563 <https://doi.org/10.1016/j.rse.2019.111563>.

- Liang, X., Li, P., Wang, J., Shun Chan, F.K., Togtokh, C., Ochir, A., Davaasuren, D., 2021. Research Progress of desertification and its prevention in Mongolia. *Sustainability* 13, 6861. <https://doi.org/10.3390/su13126861>.
- Linnér, H., Messing, I., 2012. Agricultural land needs protection. *Acta Agriculturae Scandinavica, section B — Soil & Plant. Science* 62, 706–710. <https://doi.org/10.1080/09064710.2012.697574>.
- Liu, Q., Zhang, Q., Yan, Y., Zhang, X., Niu, J., Svenning, J.-C., 2020. Ecological restoration is the dominant driver of the recent reversal of desertification in the mu Us Desert (China). *J. Clean. Prod.* 268, 122241 <https://doi.org/10.1016/j.jclepro.2020.122241>.
- Meng, X., Gao, X., Li, Sen, Li, Shengyu, Lei, J., 2021. Monitoring desertification in Mongolia based on Landsat images and Google earth engine from 1990 to 2020. *Ecol. Indic.* 129, 107908 <https://doi.org/10.1016/j.ecolind.2021.107908>.
- Na, R., Du, H., Na, L., Shan, Y., He, H.S., Wu, Z., Zong, S., Yang, Y., Huang, L., 2019. Spatiotemporal changes in the Aeolian desertification of Hulunbair grassland and its driving factors in China during 1980–2015. *CATENA* 182, 104123. <https://doi.org/10.1016/j.catena.2019.104123>.
- Pekel, J., Cottam, A., Gorelick, N., Belward, A., 2016. High-resolution mapping of global surface water and its long-term changes. *Nature* 540, 418–422. <https://doi.org/10.1038/nature20584>.
- Pueyo, Y., Moret-Fernández, D., Saiz, H., Bueno, C., Alados, C., 2013. Relationships between plant spatial patterns, water infiltration capacity, and plant community composition in semi-arid Mediterranean ecosystems along stress gradients. *Ecosystems* 16, 452–466. <https://doi.org/10.1007/s10021-012-9620-5>.
- Qi, K., Zhu, J., Zheng, X., Wang, G., Li, M., 2023. Impacts of the world's largest afforestation program (three-north afforestation program) on desertification control in sandy land of China. *GIScience & Remote Sensing* 60, 2167574. <https://doi.org/10.1080/15481603.2023.2167574>.
- Ren, Y., Zhang, B., Chen, X., Liu, X., 2024. Analysis of spatial-temporal patterns and driving mechanisms of land desertification in China. *Sci. Total Environ.* 909, 168429 <https://doi.org/10.2139/ssrn.4563721>.
- Rivera-Marín, D., Dash, J., Ogutu, B., 2022. The use of remote sensing for desertification studies: a review. *J. Arid Environ.* 206, 104829 <https://doi.org/10.1016/j.jaridenv.2022.104829>.
- Saizen, I., Maekawa, A., Yamamura, N., 2010. Spatial analysis of time-series changes in livestock distribution by detection of local spatial associations in Mongolia. *Appl. Geogr.* 30, 639–649. <https://doi.org/10.1016/j.apgeog.2010.01.002>.
- Shao, W., Wang, Q., Guan, Q., Zhang, J., Yang, X., Liu, Z., 2023. Environmental sensitivity assessment of land desertification in the Hexi corridor. *China. CATENA* 220, 106728. <https://doi.org/10.1016/j.catena.2022.106728>.
- Turner, M.D., Davis, D.K., Yeh, E.T., Hiernaux, P., Loizeaux, E.R., Fornof, E.M., Rice, A. M., Suiter, A.K., 2023. Great green walls: hype, myth, and science. *Annu. Rev. Environ. Resour.* 48, 263–287. <https://doi.org/10.1146/annurev-environ-112321-111102>.
- United Nations, 1994. *United Nations Convention to Combat Desertification in those Countries Experiencing Serious Drought and/or Desertification Particularly in Africa*.
- United Nations, 2015. *Transforming our World: The 2030 Agenda for Sustainable Development*, 70/1. A/RES/.
- Veldman, J., Overbeck, G., Negreiros, D., Mahy, G., Le Stradic, S., Fernandes, G., Durigan, G., Buisson, E., Putz, F., Bond, W., 2015. Where tree planting and Forest expansion are bad for biodiversity and ecosystem services. *BioScience* 65, 1011–1018. <https://doi.org/10.1093/biosci/biv118>.
- Wang, J., Wei, H., Cheng, K., Ochir, A., Davaasuren, D., Li, P., Shun Chan, F.K., Nasanbat, E., 2020. Spatio-temporal pattern of land degradation from 1990 to 2015 in Mongolia. *Environmental Development, Resources Use, Ecosystem Restoration and Green Development* 34, 100497. <https://doi.org/10.1016/j.envdev.2020.100497>.
- Wang, J., Wei, H., Cheng, K., Ochir, A., Shao, Y., Yao, J., Wu, Y., Han, X., Davaasuren, D., Chonokhuu, S., Zhou, Y., Zhang, M., Cao, X., Gao, M., Zhu, J., Li, Y., Li, Q., Liang, X., Li, K., 2022. Updatable dataset revealing decade changes in land cover types in Mongolia. *Geosci. Data J.* 9, 341–354. <https://doi.org/10.1002/gdj3.149>.
- Wang, J.F., Xu, C.D., 2017. Geodetectors: principles and perspectives. *J. Geogr.* 72, 116–134. <https://doi.org/10.11821/dlxb201701010>.
- Wang, X., Ge, Q., Geng, X., Wang, Zhaosheng, Gao, L., Bryan, B.A., Chen, Shengqian, Su, Y., Cai, D., Ye, J., Sun, J., Lu, H., Che, H., Cheng, H., Liu, H., Liu, B., Dong, Z., Cao, S., Hua, T., Chen, Siyu, Sun, F., Luo, G., Wang, Zhenting, Hu, S., Xu, D., Chen, M., Li, D., Liu, F., Xu, X., Han, D., Zheng, Y., Xiao, F., Li, X., Wang, P., Chen, F., 2023a. Unintended consequences of combating desertification in China. *Nat. Commun.* 14, 1139. <https://doi.org/10.1038/s41467-023-36835-z>.
- Wang, Y., Xu, D., Li, L., 2023c. Assessing the influences of natural and human factors upon desertification vulnerability in northern China during 1985–2010. *CATENA* 233, 107529. <https://doi.org/10.1016/j.catena.2023.107529>.
- Wang, Z., Shi, Y., Zhang, Y., 2023b. Review of desert mobility assessment and desertification monitoring based on remote sensing. *Remote Sens.* 15, 4412. <https://doi.org/10.3390/rs15184412>.
- Wei, H., Wang, J., Cheng, K., Li, G., Ochir, A., Davaasuren, D., Chonokhuu, S., 2018. Desertification information extraction based on feature space combinations on the Mongolian plateau. *Remote Sens.* 10, 1614. <https://doi.org/10.3390/rs10101614>.
- Wei, H., Wang, J., Han, B., 2020. Desertification information extraction along the China–Mongolia Railway supported by multisource feature space and geographical zoning modeling. *IEEE J. Select. Top. Appl. Earth Observ. Remote Sens.* 13, 392–402. <https://doi.org/10.1109/JSTARS.2019.2962830>.
- Wei, W., Zhao, Y., Han, F., 2017. Adaptive clustering algorithm based on max-min distance and Bayesian decision theory. *IAENG Int. J. Comput. Sci.* 44, 180–187.
- Wessels, K., Prince, S., Frost, P., Van, Z., 2004. Assessing the effects of human-induced land degradation in the former homelands of northern South Africa with a 1 km AVHRR NDVI time-series. *Remote Sens. Environ.* 91, 47–67. <https://doi.org/10.1016/j.rse.2004.02.005>.
- Xiao, J., Shen, Y., Tateishi, R., Bayaer, W., 2006. Development of topsoil grain size index for monitoring desertification in arid land using remote sensing. *Int. J. Remote Sens.* 27, 2411–2422. <https://doi.org/10.1080/01431160600554363>.
- Xie, L., Zhong, J., Chen, F., Cao, F., Li, J., Wu, L., 2015. Evaluation of soil fertility in the succession of karst rocky desertification using principal component analysis. *Solid Earth* 6, 515–524. <https://doi.org/10.5194/se-6-515-2015>.
- Xing, M., Yao, F., Zhang, J., Meng, X., Jiang, L., Bao, Y., 2022. Data reconstruction of daily MODIS chlorophyll-a concentration and spatio-temporal variations in the northwestern Pacific. *Sci. Total Environ.* 843, 156981 <https://doi.org/10.1016/j.scitotenv.2022.156981>.
- Xu, E., Zhang, H., Li, M., 2015. Object-based mapping of karst rocky desertification using a support vector machine. *Land Degrad. Dev.* 26, 158–167. <https://doi.org/10.1002/ldr.2193>.
- Xu, S., Wang, J., Altansukh, O., Chuluun, T., 2023. Spatial-temporal pattern of desertification in the Selenge River basin of Mongolia from 1990 to 2020. *Front. Environ. Sci.* 11, 1125583. <https://doi.org/10.3389/fenvs.2023.1125583>.
- Zhai, J., Wang, L., Liu, Y., Wang, C., Mao, X., 2023. Assessing the effects of China's three-north shelter Forest program over 40 years. *Sci. Total Environ.* 857, 159354 <https://doi.org/10.1016/j.scitotenv.2022.159354>.
- Zhang, C., Wang, X., Li, J., Hua, T., 2020. Identifying the effect of climate change on desertification in northern China via trend analysis of potential evapotranspiration and precipitation. *Ecol. Indic.* 112, 106141 <https://doi.org/10.1016/j.ecolind.2020.106141>.
- Zhang, J., Guan, Q., Du, Q., Ni, F., Mi, J., Luo, H., Shao, W., 2022. Spatial and temporal dynamics of desertification and its driving mechanism in Hexi region. *Land Degrad. Dev.* 33, 3539–3556. <https://doi.org/10.1002/ldr.4407>.
- Zhang, Y., Hu, Y., Han, Y.Q., W. S., 2021. Spatial distribution and evolution of major global ecological degradation zones and research hotspots. *J. Ecol.* 41, 7599–7613. <https://doi.org/10.5846/stxb202002150260>.
- Zhang, Y., Wang, J., Ochir, A., Chonokhuu, S., Togtokh, C., 2023. Dynamic evolution of spring sand and dust storms and cross-border response in Mongolian plateau from 2000 to 2021. *Int. J. Digit. Earth* 16, 2341–2355. <https://doi.org/10.1080/17538947.2023.2224088>.
- Zhang, Z., Huisingh, D., 2018. Combating desertification in China: monitoring, control, management and revegetation. *J. Clean. Prod.* 182, 765–775. <https://doi.org/10.1016/j.jclepro.2018.01.233>.
- Zhao, Y., Gao, G., Qin, S., Yu, M., Ding, G., 2019. Progress of research on desertification monitoring and evaluation indicators. *Arid Zone Resour. Environ.* 33, 81–87. <https://doi.org/10.13448/j.cnki.jalre.2019.142>.
- Zhao, Y., Yang, S., Liu, L., Jia, X., Han, L., Yuan, X., Zhao, M., Zhang, P., 2023. Variations and driving mechanisms of desertification in the southeast section of the China–Mongolia–Russia economic zone. *Sci. Total Environ.* 887, 164004 <https://doi.org/10.1016/j.scitotenv.2023.164004>.
- Zheng, X., Lv, N., Zhang, L., 2023. Zero growth assessment of land degradation - a case study on the Mongolian plateau. *J. Ecol.* 1–13 <https://doi.org/10.20103/j.stxb.202212223645>.
- Zhou, Y., Zhang, L., Xiao, J., Williams, C.A., Vitkovskaya, I., Bao, A., 2019. Spatiotemporal transition of institutional and socioeconomic impacts on vegetation productivity in Central Asia over last three decades. *Sci. Total Environ.* 658, 922–935. <https://doi.org/10.1016/j.scitotenv.2018.12.155>.
- Zhu, Y., Zhang, J., Zhang, Y., Qin, S., Shao, Y., Gao, Y., 2019. Responses of vegetation to climatic variations in the desert region of northern China. *CATENA* 175, 27–36. <https://doi.org/10.1016/j.catena.2018.12.007>.